TOPICS IN EARLY UNIVERSE COSMOLOGY

by

Fernando Salviatto Zago

Bachelor of Science, University of São Paulo (2010)

Submitted to the Graduate Faculty of

the Kenneth P. Dietrich School of Arts and Sciences in partial

fulfillment

of the requirements for the degree of

Doctor of Philosophy

University of Pittsburgh

2019

UNIVERSITY OF PITTSBURGH

DIETRICH SCHOOL OF ARTS AND SCIENCES

This dissertation was presented

by

Fernando Salviatto Zago

It was defended on

April 29th 2019

and approved by

Arthur Kosowsky, Professor, Dept. of Physics and Astronomy, University of Pittsburgh

Daniel Boyanovsky, Professor, Dept. of Physics and Astronomy, University of Pittsburgh

Adam Leibovich, Professor, Dept. of Physics and Astronomy, University of Pittsburgh

Jeffrey Newman, Professor, Dept. of Physics and Astronomy, University of Pittsburgh

William Kinney, Professor, Dept. of Physics, State University of New York at Buffalo

Dissertation Director: Arthur Kosowsky, Professor, Dept. of Physics and Astronomy, University of Pittsburgh

TOPICS IN EARLY UNIVERSE COSMOLOGY

Fernando Salviatto Zago, PhD

University of Pittsburgh, 2019

Probes of the cosmic microwave background have revealed a spatially flat and highly isotropic early Universe, seeded with small gaussian primordial perturbations characterized by a nearly scale-invariant power spectrum. The physics responsible for sourcing this early state, however, is still a subject of debate and remains largely speculative. This work explores theoretical and computational methods with the aim of further understanding the physical mechanisms which were at play during this early phase of our Universe.

An early period of accelerated cosmic expansion, known as inflation, is one possible scenario which has been proposed to account for the above-mentioned large-scale properties of our Universe. It is therefore of interest to place observational constraints on inflationary dynamics in order to better understand its physical origin. To that end, in the first original portion of this work, we employ quantum mechanical inverse-scattering techniques with the aim of shedding light on the stress-energy responsible for this proposed early inflationary state. In particular, we demonstrate a numerical reconstruction of two simulated inflationary histories assuming perfect knowledge of their corresponding observables. Taking stock of these results, we then briefly discuss the application of this technique to more realistic cases incorporating uncertainties and limited access to cosmological data.

Subsequently, in the second original portion of this thesis, we investigate the effects of quantum particle production on the cosmic evolution. This effect is particularly relevant for models of the very early Universe, when the energy density generated through this process may back-react on the cosmological expansion. Here we demonstrate a numerical solution to the back-reaction problem in regimes dominated by particle production. Finally, we discuss

the relevance of quantum particle production to bounce and inflationary models of the early Universe.

TABLE OF CONTENTS

LIST OF TABLES

LIST OF FIGURES

LIST OF EQUATIONS

PREFACE

I wish to thank all of those who shared, in one way or another, this journey with me. I am particularly grateful to my advisor, Arthur Kosowsky, for his support and guidance throughout these years. Thank you for patiently helping me remain focused, and for instilling in me an appreciation for the bigger picture.

I would also like to extend my deepest gratitude to the members of my committee: Adam Leibovich, Jeffrey Newman, William Kinney, and especially Daniel Boyanovsky. Thank you for your valuable feedback and stimulating discussions. I am also extremely thankful to Sandhya Rao for her mentorship, to David Turnshek for his kind support, Regina Schulte-Ladbeck for her helpful advice, and Rachel Bezanson for taking the time to brief and advise me about the post-doctoral application season.

I am greatly indebted to Leyla Hirschfeld and Robert Breeze, whose expertise and patience were instrumental in helping me navigate the different aspects of graduate school, and to Jim Stango, for his most helpful assistance in the classroom setting.

I must also thank my friends and colleagues, who each in their own ways contributed to make my experience in Pittsburgh ever more enjoyable. Special thanks belong to Ciro Bertolucci, Danilo Carandina, Corey Dominick, Paulo Felisberto, Barmak Shams Es Haghi, Hector Martinez Rodriguez, James Rotella, Bradley Slezak, Xing Wang, Daniel Wiegand, and Rongpu Zhou.

Finally, I would like to thank my family. This work would have not been possible without the nurturing support of my parents and sister, Luiz Carlos Zago, Maria Angélica Salviatto Zago, and Nathália Salviatto Zago, and the caring counsel of my parents-in-law, Francisco Carranza Romero and Hye Sun Ko. Most importantly, I would like to thank my loving wife, Ñusta Carranza Ko, for her continuous encouragement and for believing in me at every step

of the way. To my daughter, Marie Carranza Zago, for bringing so much joy into my life.

1.0 INTRODUCTION

In this Chapter we review the theoretical framework which underpins most of the modern research on the physics of the early Universe. Despite not constituting original work, the material presented here is fundamental for a complete understanding of Chapters 2 and 3. Unless otherwise stated, the content of this Chapter follows the standard literature on General Relativity [1–3], Cosmology [4–6], and Quantum Field Theory on Curved Spacetimes [7,8].

1.1 FRIEDMANN-LEMAÎTRE-ROBERTSON-WALKER SPACETIMES

The large-scale evolution of the Universe is governed by the gravitational interaction as described by the Einstein equations

$$R_{ab} - \frac{1}{2} R\, g_{ab} + \Lambda\, g_{ab} = 8\pi G\, T_{ab}\,. \tag{1.1}$$

Here g_{ab} denotes the spacetime metric, while R_{ab} and $R = g^{ab}R_{ab}$ correspond to the Ricci tensor and the Ricci scalar, respectively. The quantity Λ represents the cosmological constant, and G stands for the universal gravitational constant. Finally, T_{ab} encapsulates the energy-momentum of each material component populating the Universe.

At its largest scales, the Universe is statistically homogeneous and isotropic [9–11], and is modeled most appropriately by the Friedmann-Lemaître-Robertson-Walker (FLRW) metric. In terms of the comoving coordinates of freely falling observers this metric is expressed by the following line element:

$$\mathrm{d}s^2 = g_{ab}\mathrm{d}x^a\mathrm{d}x^b = -\mathrm{d}t^2 + a^2(t) g_{ij}\mathrm{d}x^i\mathrm{d}x^j\,, \tag{1.2}$$

with spatial sections of constant curvature described by

$$g_{ij}\mathrm{d}x^i\mathrm{d}x^j = \frac{\mathrm{d}r^2}{1-Kr^2} + r^2\mathrm{d}\theta^2 + r^2\sin^2\theta\,\mathrm{d}\varphi^2\,. \tag{1.3}$$

The scale factor $a(t)$ featuring above describes the cosmological expansion history, while $K = -1,\ 0,\ +1$ corresponds to the curvature parameter of an open, flat, and closed Universe, respectively. Furthermore, the non-vanishing components of the Ricci tensor associated with this metric are

$$R_{00}(t) = 3\Big[\dot{H}(t) + H^2(t)\Big]g_{00} \tag{1.4a}$$

$$R_{ij}(t) = \Big[\dot{H}(t) + 3H^2(t) + 2K/a^2(t)\Big]g_{ij}\,, \tag{1.4b}$$

and the Ricci scalar is is given by

$$R(t) = 6\Big[\dot{H}(t) + 2H^2(t) + K/a^2(t)\Big]\,, \tag{1.5}$$

where

$$H(t) \equiv \frac{\dot{a}(t)}{a(t)} \tag{1.6}$$

is the Hubble parameter, and overdots indicate differentiation with respect to the proper time t. We will often find it convenient to substitute the time coordinate employed above by the conformal time η defined by the following differential relation:

$$\mathrm{d}\eta \equiv \frac{\mathrm{d}t}{a(t)}\,. \tag{1.7}$$

In terms of this quantity, the Hubble parameter can be expressed as

$$H(\eta) = \frac{a'(\eta)}{a^2(\eta)}\,, \tag{1.8}$$

where the prime indicates differentiation with respect to η. It is worth noting that the integral form of Eq. (1.7) also defines the comoving cosmological horizon

$$\eta = \int \frac{\mathrm{d}t}{a(t)} \tag{1.9}$$

which encodes the typical size of causally connected regions.

Component	**Parameter**	**Energy Density**
Radiation	$w_{\rm R} = \frac{1}{3}$	$\rho_{\rm R}(t) \propto a^{-4}(t)$
Pressureless Matter	$w_{\rm M} = 0$	$\rho_{\rm M}(t) \propto a^{-3}(t)$
Cosmological Constant	$w_\Lambda = -1$	$\rho_\Lambda(t) \propto$ const.

Table 1: The typical perfect fluid components featuring in FLRW models, along with their respective equation of state parameters, and energy densities expressed in terms of the cosmic scale factor. Notice that the energy density of matter scales inversely with the comoving volume specified by the scale factor, while the energy density of radiation scales with an additional inverse power of the scale factor induced by the cosmological redshift. The energy density associated with the cosmological constant remains unchanged, and does not dilute as the cosmic expansion unfolds.

Statistical homogeneity and isotropy also implies that the energy-momentum tensor T_{ab} encodes a mixture of perfect fluids for which the total energy density and pressure are given, respectively, by

$$\rho(t) = T_{00} = \sum_n \rho_n(t) \tag{1.10a}$$

$$P(t) = \frac{1}{3} g^{ij} T_{ij} = \sum_n P_n(t)\,, \tag{1.10b}$$

where the summations run over every component of the mixture. In addition, it follows from the covariant conservation of T_{ab} that each of these components satisfies the cosmological continuity equation

$$\dot{\rho}_n(t) + 3H(t)\Big[\rho_n(t) + P_n(t)\Big] = 0\,. \tag{1.11}$$

A good approximation for most perfect fluids of interest consists in assuming that the following equation of state holds:

$$P_n(t) = w_n\, \rho_n(t)\,, \tag{1.12}$$

where w_n is referred to as the equation of state parameter. Some of the typical perfect fluid components featuring in FLRW models fall in this category, most notably: radiation, described by $w_{\rm R} = \frac{1}{3}$; and pressureless matter, for which $w_{\rm M} = 0$. Interestingly, the contributions due to the cosmological constant Λ can also be modeled by a perfect fluid with equation of state parameter given by $w_\Lambda = -1$. For these cases, Eqs. (1.11) and (1.12) can be solved exactly, the results of which are collected in Table 1.

In view of the above considerations, Eq. (1.1) reduces to the usual Friedmann equations

$$H^2(t) = \frac{8\pi G}{3}\rho(t) + \frac{\Lambda}{3} - \frac{K}{a^2(t)} \tag{1.13a}$$

$$\dot{H}(t) + H^2(t) = -\frac{8\pi G}{6}\Big[\rho(t) + 3P(t)\Big] + \frac{\Lambda}{3}\,, \tag{1.13b}$$

which govern the expansion of the Universe and the evolution of its energy-momentum content. In what follows in Section 1.2, we briefly review the current constraints on the Universe's curvature and composition, and summarize the cosmological history these observations imply through Eqs. (1.13). Most importantly, we discuss how these very observations suggest the need for an extension of the standard FLRW cosmological model at very early times.

1.2 THE ΛCDM MODEL AND ITS PROBLEMS

In the past decades, probes of the cosmic microwave background [9,10], as well as surveys of the distribution of galaxies and galaxy clusters [11,12], and gravitational lensing studies [13, 14] have made substantial progress in determining the large-scale properties of our Universe. In the context of a FLRW cosmological model, these remarkable observations translate into constraints on the density parameters

$$\boldsymbol{\Omega}_n(t) \equiv \frac{8\pi G}{3}\frac{\rho_n(t)}{H^2(t)}\,, \quad \boldsymbol{\Omega}_\Lambda(t) \equiv \frac{1}{3}\frac{\Lambda}{H^2(t)}\,, \quad \text{and} \quad \boldsymbol{\Omega}_K(t) \equiv -\frac{K}{a^2(t)H^2(t)}\,, \tag{1.14}$$

which parametrize the relative dominance of each contribution featuring on the right-hand side of Eq. (1.13a) throughout cosmic history. The inferred present values for each of these

Component	Parameter	Present Value
Curvature	$\boldsymbol{\Omega}_K$	0.0008 ± 0.0013
Radiation	$\boldsymbol{\Omega}_{\mathrm{R}}$	$9.17 \pm 1.90 \times 10^{-6}$
Baryonic Matter	$\boldsymbol{\Omega}_{\mathrm{M}}$	0.0486 ± 0.0010
Dark Matter	$\boldsymbol{\Omega}_{\mathrm{DM}}$	0.2589 ± 0.0057
Dark Energy	$\boldsymbol{\Omega}_{\Lambda}$	0.6911 ± 0.0062

Table 2: The present cosmological density parameters measured by the Planck Collaboration reveal a spatially flat Universe dominated by dark energy and cold dark matter. All measured values have been either reproduced from Ref. [9] or computed from results reported therein.

quantities are shown in Table 2, revealing a spatially flat Universe dominated by its cosmological constant and cold dark matter content. This particular FLRW model is labeled by the acronym ΛCDM, after its current dominant components.

The cosmic history implied by the ΛCDM density parameters is depicted schematically in Figure 1. At early times the cosmic expansion is dictated by $\boldsymbol{\Omega}_{\mathrm{R}}$, marking out the radiation era. Lasting from $t \approx 10^{-12}\,\mathrm{s}$ to $t \approx 60\,\mathrm{kyr}$, this phase is initially characterized by a primordial plasma of fundamental particles which progressively cools down to form nucleons and trace amounts of the lightest elements [16]. As the Universe expands, the combined contributions from $\boldsymbol{\Omega}_{\mathrm{M}}$ and $\boldsymbol{\Omega}_{\mathrm{DM}}$ eventually come to dominate the cosmic evolution, establishing the matter era. It is during this phase, at $t \approx 300\,\mathrm{kyr}$, that the opaque plasma permeating the Universe becomes transparent as nuclei and electrons combine into neutral atoms in an event referred to as "recombination" [17]. The radiation released at this point is detected today as the cosmic microwave background (hereafter termed CMB). Towards the end of the matter era, the Universe has been reionized by the first stars and quasars [18] and structure formation is well underway [19]. At $t \approx 9.4\,\mathrm{Gyr}$ the matter components have

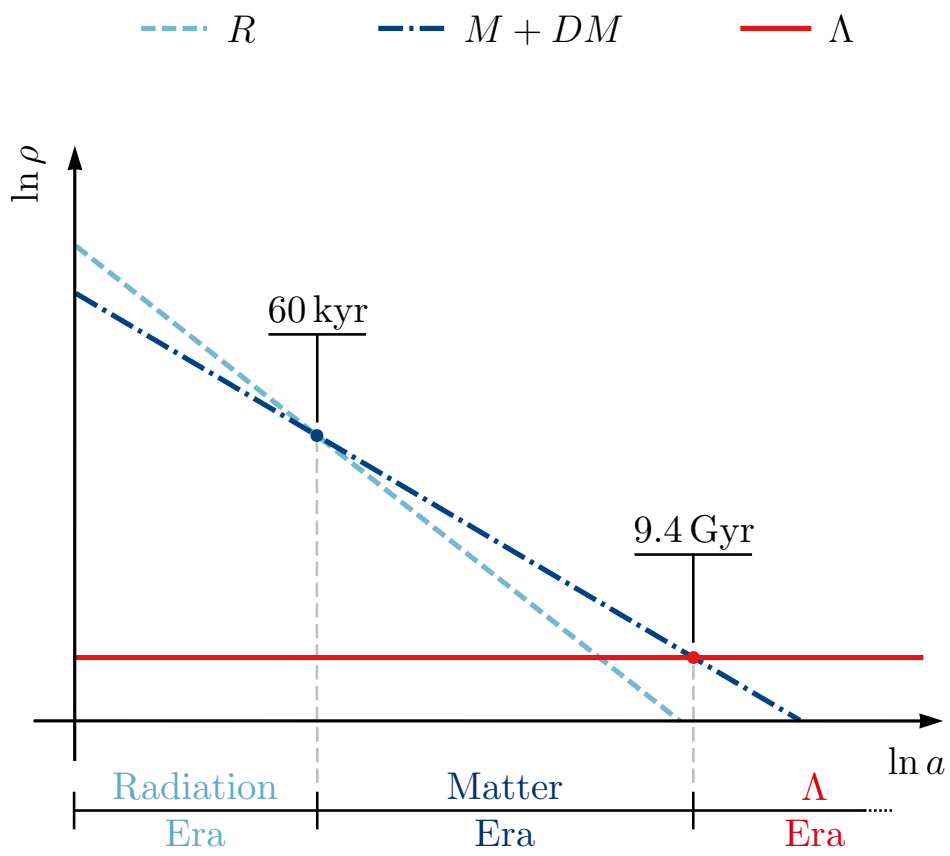

Figure 1: Schematic illustration of the cosmic history for the ΛCDM Universe. The radiation era lasts from $t \approx 10^{-12}\,\mathrm{s}$ to $t \approx 60\,\mathrm{kyr}$, and is followed by the matter era which lasts until $t \approx 9.4\,\mathrm{Gyr}$. Once the matter and radiation components have been sufficiently diluted, the cosmological constant emerges as the dominant component in what is called the Λ era.

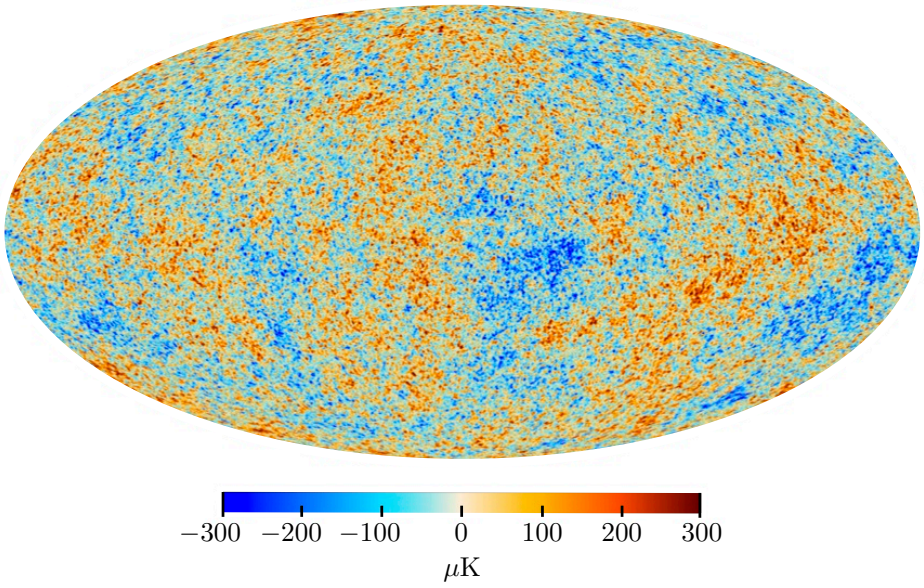

Figure 2: The CMB temperature anisotropy map produced by the Planck Collaboration [15]. Different colors correspond to fluctuations of approximately 1 part in 10^5 around the average temperature of $T \approx 2.72\,\mu$K. In a pure ΛCDM framework, points characterized by an angular separation of $\theta \geq 2^\circ$ belong to causally disconnected regions. Still, the above map shows that the CMB sky is highly isotropic, implying that the entire surface it describes was causally connected in the past.

become sufficiently diluted for $\boldsymbol{\Omega}_\Lambda$ to emerge as the dominant component driving the cosmic expansion, initiating the Λ era [20].

Despite its success in explaining nearly 13.8 Gyr of cosmic history, the ΛCDM framework fails to provide a satisfactory description of the Universe for $t \lesssim 10^{-12}$ s. This is evidenced by the model's fine-tuning and consistency problems, all of which can be traced back to the Universe's conditions at very early times. The flatness problem, for instance, follows from the general result that a flat FLRW cosmology corresponds to an unstable equilibrium solution of the Friedmann equations. As a consequence, any small deviation from flatness at early times should have been greatly amplified by the Universe's expansion. This result is in contrast with current observations which have established $\boldsymbol{\Omega}_K = 0$ within a percent on large scales (see Table 2). In the context of FLRW cosmologies, such a small present value for the curvature parameter implies an extremely fine-tuned initial state for the Universe – an explanation which is widely regarded as unsatisfactory from a physical point of view. Another example is the horizon problem, which is associated with the temperature correlations exhibited by the CMB on large angular separations. In a pure ΛCDM framework, points on the surface of last scattering characterized by an angular separation of $\theta \geq 2^\circ$ belonged to causally disconnected regions at the time of recombination, and consequently would not have had enough time to reach thermal equilibrium. Therefore, the isotropy observed on the CMB temperature map (see Figure 2) implies the existence of correlations on scales larger than the causal horizon which cannot be accounted for in the standard ΛCDM model.

The fine-tuning and consistency problems discussed above suggest the need for an extension of the standard ΛCDM cosmological model at very early times [21]. An early period of accelerated cosmic expansion, known as inflation, is one possible scenario which has been proposed to address these issues. Below, in Section 1.3, we discuss the general features of an early inflationary phase, as well as its modeling through the dynamics of scalar fields.

1.3 INFLATION AND SCALAR FIELDS

Although initially introduced as a mechanism to dilute unobserved relic particles (e.g., magnetic monopoles) which could have been produced in the high-energy environment of the primordial Universe, it was soon realized that a period of inflationary expansion could also successfully resolve the long-standing flatness and horizon problems of the standard ΛCDM model [22, 23]. In this section we review the general features of cosmological inflation and discuss how such a phase can be modeled through the dynamics of scalar fields.

In order to understand how inflation solves both the horizon and the flatness problems, we assume that for $t \lesssim 10^{-12}\,\mathrm{s}$ the Universe is dominated by an unknown form of stress-energy characterized by the density parameter $\boldsymbol{\Omega}_\Phi$, and possibly by the curvature density parameter $\boldsymbol{\Omega}_K$. In this context, the Friedmann Eqs. (1.13) can be recast as follows [24]:

$$\boldsymbol{\Omega}_\Phi + \boldsymbol{\Omega}_K = 1 \tag{1.15a}$$

$$\frac{d\boldsymbol{\Omega}_\Phi}{d\ln a} = (1 + 3w_\Phi)\,(\boldsymbol{\Omega}_\Phi - 1)\,\boldsymbol{\Omega}_\Phi\,, \tag{1.15b}$$

where we have made use of Eq. (1.12) to introduce the equation of state parameter w_Φ. At this point we can impose the condition for inflationary expansion ($\ddot{a} > 0$, or $w_\Phi < -\frac{1}{3}$) and analyze its consequences. First we notice that Eqs. (1.15) imply that an inflationary phase drives $\boldsymbol{\Omega}_\Phi \longrightarrow 1$ and $\boldsymbol{\Omega}_K \longrightarrow 0$, which is to say that the Universe is driven towards flatness. Second, it is easy to show that whenever $\boldsymbol{\Omega}_K \longrightarrow 0$ the following inequality holds:

$$\frac{d\eta}{d\ln a} < 0\,. \tag{1.16}$$

In other words, the comoving cosmological horizon shrinks when the Universe undergoes a phase of accelerated expansion, making the large-angle CMB correlations possible. Thus, an early inflationary scenario is capable of eliminating the contradictions present in the standard ΛCDM framework at the cost of postulating an epoch dominated by an unusual form of stress-energy. Below we review the simplest implementation of such a scenario through the dynamics of a single scalar field minimally coupled to gravity.

The action for a self-interacting scalar field $\Phi(t, \mathbf{x})$, hereafter referred to as the inflaton

field, can be expressed generically as

$$S = -\frac{1}{2}\int \sqrt{-g}\,\mathrm{d}^4x\Big[\big(\nabla_a\Phi\big)g^{ab}\big(\nabla_b\Phi\big) - V(\Phi)\Big]\,, \tag{1.17}$$

where ∇_a is the covariant derivative, $g = \det(g_{ab})$, and the functional $V(\Phi)$ encapsulates all the unknown self-interacting properties of the field under consideration. Applying the variational principle to this action yields the equation of motion

$$\left[\Box - \frac{\partial V}{\partial \Phi}\right]\Phi(t,\,\mathbf{x}) = 0\,, \tag{1.18}$$

where $\Box = g^{ab}\nabla_a\nabla_b$ is the d'Alembert operator associated with the underlying spacetime. Similarly, the expression for the energy-momentum tensor T_{ab} associated with the inflaton field can be constructed by varying the action in Eq. (1.17) with respect to the metric g_{ab}, yielding

$$T_{ab} = \big(\nabla_a\Phi\big)\big(\nabla_b\Phi\big) - \frac{1}{2}g_{ab}\Big[\big(\nabla^c\Phi\big)\big(\nabla_c\Phi\big) + V(\Phi)\Big]\,. \tag{1.19}$$

This result simplifies considerably for the case of a homogeneous field, matching the energy-momentum tensor of a perfect fluid with energy density and pressure given by

$$\rho_\Phi(t) = \frac{1}{2}\dot{\Phi}^2(t) + V(\Phi) \tag{1.20a}$$

$$P_\Phi(t) = \frac{1}{2}\dot{\Phi}^2(t) - V(\Phi)\,. \tag{1.20b}$$

It follows from Eqs. (1.12) and (1.20) that the inflaton field possesses an evolving equation of state parameter, w_Φ. Most importantly, for the limiting case in which $\dot{\Phi}^2 \ll V(\Phi)$, the equation of state parameter assumes a form equivalent to that of cosmological constant, i.e., $w_\Phi \simeq -1$. This is referred to as the slow-roll phase of the field evolution, and is typically parametrized by the slow-roll parameter

$$\epsilon \equiv -\frac{\dot{H}(t)}{H^2(t)} = -\frac{H'(\eta)}{a^2(\eta)H^2(\eta)}\,. \tag{1.21}$$

Inflation happens precisely during this phase, when the scale factor experiences quasi-exponential growth. The amount of expansion produced during slow-roll is commonly quan-

tified by the number of e-foldings

$$N = \ln\left(\frac{a_{\rm end}}{a}\right), \tag{1.22}$$

where $a_{\rm end}$ corresponds to the scale factor at the end of inflation. This definition is essentially that of a regressive countdown, and expresses that for a given value of N the scale factor has still to grow by a factor of e^N before inflation ends at $N = 0$. Typical inflation models are required to generate about 60 e-foldings in order to agree with CMB observations [25].

In this section we have summarized the motivations behind inflationary cosmology, as well as its modeling through the dynamics of a homogeneous self-interacting scalar field. Remarkably, within the inflationary paradigm, the initial density perturbations responsible for seeding the growth of structure in the Universe have a natural quantum mechanical origin. We review this important result in some detail in Sections 1.4 and 1.5 below.

1.4 QUANTIZATION OF SCALAR FIELDS IN FLRW SPACETIMES

Here we briefly review the relevant results regarding the canonical quantization of scalar fields in FLRW spacetimes (see, e.g., [7,8]). We restrict ourselves to the case of a free scalar fields $\Phi(t, \mathbf{x})$ of arbitrary mass and curvature coupling. The action for such a field is given by

$$S = -\frac{1}{2}\int \sqrt{-g}\,\mathrm{d}^4x\Big[\big(\nabla_a\Phi\big)g^{ab}\big(\nabla_b\Phi\big) + m^2\Phi^2 + \xi R\Phi^2\Big], \tag{1.23}$$

where ∇_a is the covariant derivative, $g = \det(g_{ab})$, m is the field mass, and ξ is the field coupling to the spacetime curvature. Applying the variational principle to this action yields the equation of motion

$$\Big[\Box - m^2 - \xi R(t)\Big]\Phi(t, \mathbf{x}) = 0\,, \tag{1.24}$$

where $\Box = g^{ab}\nabla_a\nabla_b$ is the d'Alembert operator associated with the spacetime. Due to the homogeneity and isotropy of the background FLRW metric, the solutions of Eq. (1.24) can be separated into purely temporal and spatial parts. As a consequence, the quantized field

operator can be written as

$$\hat{\Phi}(t,\,\mathbf{x}) = a^{-3/2}(t)\int \mathrm{d}\mu(k)\Big[a_{\mathbf{k}} f_k(t) Y_{\mathbf{k}}(\mathbf{x}) + a^{\dagger}_{\mathbf{k}} f^{*}_k(t) Y^{*}_{\mathbf{k}}(\mathbf{x})\Big]\,, \tag{1.25}$$

where the raising and lowering operators $a^{\dagger}_{\mathbf{k}}$ and $a_{\mathbf{k}}$ satisfy the canonical commutation relations

$$\Big[a_{\mathbf{k}}\,, a^{\dagger}_{\mathbf{k}'}\Big] = \delta_{\mathbf{k},\,\mathbf{k}'}\,, \tag{1.26}$$

and $\mathrm{d}\mu(k)$ is a geometry-dependent integration measure given by

$$\int \mathrm{d}\mu(k) = \begin{cases} \displaystyle\sum_{k=1}^{\infty} k^2\,, & \text{for } K = +1 \\ \displaystyle\int_0^{\infty} k^2\,\mathrm{d}k\,, & \text{for } K = 0,\,-1\,. \end{cases} \tag{1.27}$$

The functions $Y_{\mathbf{k}}(\mathbf{x})$ and $f_k(t)$ contain the spatial and temporal dependence of each $\mathbf{k}$-mode. The harmonic functions $Y_{\mathbf{k}}(\mathbf{x})$ are eigenfunctions of the Laplace-Beltrami operator associated with the geometry of spatial hypersurfaces, while the mode functions $f_k(t)$ obey the harmnonic oscillator equation

$$\ddot{f}_k(t) + \Omega^2_k(t) f_k(t) = 0 \tag{1.28}$$

with the time-dependent frequency function

$$\Omega^2_k(t) = \omega^2_k(t) + \left(\xi - \frac{1}{6}\right) R(t) - \left[\frac{\dot{H}(t)}{2} + \frac{H^2(t)}{4}\right], \tag{1.29}$$

where

$$\omega_k(t) = \left[\frac{k^2}{a^2(t)} + m^2\right]^{1/2}. \tag{1.30}$$

The complex mode functions $f_k(t)$ and $f^{*}_k(t)$ also satisfy the Wronskian condition

$$f_k(t)\dot{f}^{*}_k(t) - \dot{f}_k(t) f^{*}_k(t) = i\,. \tag{1.31}$$

If Eq. (1.31) holds at some particular time t, then Eq. (1.28) guarantees it will also hold at all future times.

The quantization procedure outlined above naturally leads to the construction of the Fock space of field states. The base element of this space is the vacuum state, which is

defined as the normalized state that is annihilated by all lowering operators:

$$a_{\mathbf{k}}\,|0\rangle = 0 \quad \text{and} \quad \langle 0|0\rangle = 1\,. \tag{1.32}$$

All remaining states are generated from the vacuum by the successive application of raising operators, such as

$$|\mathbf{k}_1,\, \mathbf{k}_2,\, \ldots\rangle = a^\dagger_{\mathbf{k}_1} a^\dagger_{\mathbf{k}_2} \ldots |0\rangle\ , \tag{1.33}$$

and normalized by the requirement of mutual orthonormality. The family of field states which are spatially isotropic and homogeneous is of particular interest, as these states constitute viable sources of the FLRW metric.

The field operator $\hat{\Phi}(t,\, \mathbf{x})$ admits numerous representations of the form shown in Eq. (1.25), each of which is associated with a different mode function pertaining to the set of solutions of Eq. (1.28). These representations are related: the complex mode functions $f_k(t)$ and $h_k(t)$ belonging to any two different representations can be expressed in terms of one another through the Bogolyubov transformations

$$f_k(t) = \alpha_k h_k(t) + \beta_k h^*_k(t)\,, \tag{1.34a}$$

$$f^*_k(t) = \beta^*_k h_k(t) + \alpha^*_k h^*_k(t)\,, \tag{1.34b}$$

where α_k and β_k are known as Bogolyubov coefficients. Due to homogeneity and isotropy, these coefficients depend only on $k = |\mathbf{k}|$. Substituting these expressions into Eq. (1.25) leads to similar transformations relating the raising and lowering operators belonging to these representations:

$$a_{\mathbf{k}} = \alpha^*_k b_{\mathbf{k}} - \beta^*_k b^\dagger_{\mathbf{k}}\,, \tag{1.35a}$$

$$a^\dagger_{\mathbf{k}} = \alpha_k b^\dagger_{\mathbf{k}} - \beta_k b_{\mathbf{k}}\,, \tag{1.35b}$$

from which it follows that the Bogolyubov coefficients must satisfy

$$\big|\alpha_k\big|^2 - \big|\beta_k\big|^2 = 1 \tag{1.36}$$

in order to guarantee that the commutation relations of Eq. (1.26) are valid across all representations.

A direct consequence of Eqs. (1.35) is that the notion of vacuum is not unique for a quantized field defined on a FLRW spacetime [7, 8]. This is evident from the following simple calculation, which shows that the vacuum defined in Eq. (1.32) is not necessarily devoid of particles according to the number operator belonging to a different field representation:

$$\begin{aligned}\mathcal{N}_k &= \langle 0|b_{\mathbf{k}}^{\dagger}b_{\mathbf{k}}|0\rangle \\ &= |\alpha_k|^2\langle 0|a_{\mathbf{k}}^{\dagger}a_{\mathbf{k}}|0\rangle + |\beta_k|^2\langle 0|a_{\mathbf{k}}a_{\mathbf{k}}^{\dagger}|0\rangle \\ &= |\beta_k|^2 .\end{aligned} \tag{1.37}$$

Therefore, different choices of representation inevitably lead to distinct notions of vacuum and, consequently, to distinct notions of particle. This result is a quite general feature of quantum field theory defined on curved spacetimes. The question of whether the effects of particle production can become sufficiently pronounced to affect the evolution of the early Universe is addressed in Chapter 3.

Next, in Section 1.5, we discuss how the quantized fluctuations of the inflaton field give rise to the initial density perturbations responsible for seeding the growth of structure in the Universe. In particular, we review the observables associated with such primordial fluctuations.

1.5 GENERATION OF PRIMORDIAL PERTURBATIONS

In Section 1.3, an early inflationary phase was modeled by a homogeneous and isotropic self-interacting field $\Phi(t)$. However, a complete picture of inflation must also incorporate field fluctuations of the form $\Phi(t) + \delta\Phi(t, \mathbf{x})$, as well as their associated curvature perturbations induced on the spacetime metric. This is accomplished by employing the perturbed Einstein equations, and by expressing all relevant physical quantities in terms of gauge invariant potentials [26]. Here we will be particularly interested in the Mukhanov potential $\phi(\eta, \mathbf{x})$ which describes scalar fluctuations, and the tensorial potential $h_{ij}(\eta, \mathbf{x})$ which encodes gravitational

waves. Both of these quantities are excited during inflation, and constitute natural degrees of freedom to be quantized [27]. Below we discuss the connection between the quantized nature of $\phi(\eta, \mathbf{x})$ and $h_{ij}(\eta, \mathbf{x})$ and the generation of primordial fluctuations. In particular, we review the observable implications of this formalism, as well as current observational constraints.

We begin by analyzing the evolution of Mukhanov potential $\phi(\eta, \mathbf{x})$. In the comoving gauge, this quantity assumes the following form:

$$\phi(\eta, \mathbf{x}) = z(\eta)\, \mathcal{C}(\eta, \mathbf{x})\,, \tag{1.38}$$

where $\mathcal{C}(\eta, \mathbf{x})$ corresponds to the comoving curvature perturbation of the metric, and $z(\eta)$ is defined as

$$z(\eta) \equiv \frac{a(\eta)\sqrt{2\epsilon(\eta)}}{c_s}\,, \tag{1.39}$$

with c_s being the adiabatic sound speed during inflation. For simplicity we assume $c_s = 1$, appropriate for inflation driven by a scalar field. Furthermore, it can be shown that the quadratic action for $\phi(\eta, \mathbf{x})$ takes the form shown in Eq. (1.23) when expressed in terms of the conformal time. As a consequence, the Mukhanov potential can be quantized according to the procedure outlined in Section 1.4. The resulting field operator $\hat{\phi}(\eta, \mathbf{x})$ is described by the time-dependent mode functions $\phi_k(\eta)$ which evolve according to the Mukhanov-Sasaki equation [28, 29]:

$$\phi_k''(\eta) + \Big[k^2 - q(\eta)\Big]\phi_k(\eta) = 0\,, \tag{1.40}$$

where the primes indicate differentiation with respect to conformal time η, and the freeze-out horizon is given by

$$q(\eta) = \frac{z''(\eta)}{z(\eta)}\,. \tag{1.41}$$

Also, notice that Eq. (1.40) above is analogous to Eq. (1.28).

In general, the evolution of each mode goes through two main phases, denominated sub-horizon and super-horizon. During sub-horizon evolution, the mode wavelength is small compared to the horizon size, $k \gg q(\eta)$. From Eq. (1.40), this condition implies that each mode oscillates as in a non-expanding Universe. This allows the vacuum of $\hat{\phi}(\eta, \mathbf{x})$ to be set through the correspondence of each mode $\phi_k(\eta)$ with the positive frequency modes of

Minkowski spacetime, thus fixing

$$\phi_k(\eta) \sim \frac{1}{\sqrt{2k}} \exp\big(-ik\eta\big) \quad \text{for} \quad \eta \longrightarrow -\infty\,. \tag{1.42}$$

These initial conditions establish the well-known Bunch-Davies vacuum. As inflation unfolds $q(\eta)$ increases, and sub-horizon modes eventually become super-horizon with $k \ll q(\eta)$. In this limit, the modes $\phi_k(\eta)$ no longer propagate freely, but rather exhibit a freeze-out behavior given by

$$\phi_k(\eta) \sim A_k\, z(\eta)\,, \tag{1.43}$$

where A_k is a function of k alone, and clearly dependent on the choice of vacuum. Observationally, the freeze-out behavior described above fixes the form of the correlation function $\big\langle \hat{\phi}(\eta,\, \mathbf{x})\, \hat{\phi}(\eta,\, \mathbf{x}')\big\rangle$. It is conventional, however, to work with the dimensionless primordial power spectrum of curvature fluctuations associated with this function [30]:

$$P_{\mathcal{C}}(k) = \frac{k^3}{2\pi^2}\, |A_k|^2\ . \tag{1.44}$$

Here we note that the value of a perturbation, given by A_k for a wavenumber k, is to a good approximation fixed at horizon crossing $k \simeq q(\eta)$. Consequently, a measurement of $P_{\mathcal{C}}(k)$ constrains the evolution of the horizon crossing scale $q(\eta)$ during inflation. In the literature, measurements of the power spectrum are usually parametrized by the following functional form:

$$P_{\mathcal{C}}(k) = P_{\mathcal{C}}(k_0) \left(\frac{k}{k_0}\right)^{n_s - 1}\,, \tag{1.45}$$

where k_0 is a pivot scale, and n_s is the scalar spectral index.

Similar calculations apply to the tensor perturbations $h_{ij}(\eta,\, \mathbf{x})$ whose evolution can also be understood in terms of the freeze-out formalism discussed above. Just like the scalar mode functions, the corresponding tensor modes $h_k(\eta)$ evolve according to Eq. (1.40), with the freeze-out horizon assuming the simplified form

$$q(\eta) = \frac{a''(\eta)}{a(\eta)}\,. \tag{1.46}$$

Parameter	Measured Value
$P_{\mathcal{C}}(k_0)$	$2.141 \pm 0.049 \times 10^{-9}$
n_s	0.9667 ± 0.0040
r	< 0.07 (95%)

Table 3: The primordial power spectra parameters measured by the Planck and BICEP/Keck Collaborations reveal a nearly scale-invariant scalar power spectrum, and place an upper bound on the amplitude of the tensor power spectrum. All measured values refer to the pivot scale $k_0 = 0.05\,\mathrm{Mpc}^{-1}$ and have been reproduced from Refs. [9, 31].

As a consequence, in analogy to Eq. (1.43), the freeze-out of tensor modes is given by $h_k(\eta) \sim B_k\, a(\eta)$, and the power spectrum of primordial tensor perturbations is defined by

$$P_T(k) = 2\,\frac{k^3}{2\pi^2}\,|B_k|^2\ , \tag{1.47}$$

where the two two polarization states have been accounted for. In particular, during the slow-roll phase (ϵ nearly constant), the freeze-out horizon is given by $q(\eta) \simeq 2\,\eta^{-2}$, and an exact solution can be computed for the evolution of each mode. In this regime it can be shown that

$$P_T(k) \propto H^2\big|_{k=aH}\ , \tag{1.48}$$

where the Hubble parameter is evaluated at horizon-crossing, i.e., at $k = aH$. Therefore, a measurement of $P_T(k)$ at a particular scale also encodes information about $a(\eta)$ during inflation. Finally, observational constraints on the tensor power spectrum customarily refer to the following parametrization:

$$P_T(k) = P_T(k_0)\left(\frac{k}{k_0}\right)^{n_T}\ , \tag{1.49}$$

where n_T is known as the tensor spectral index. It is also common for the amplitude of the tensor power spectrum at the chosen pivot scale $P_T(k_0)$ to be reported in terms of the

tensor-to-scalar ratio

$$r \equiv \frac{P_T(k_0)}{P_{\mathcal{C}}(k_0)} \,. \tag{1.50}$$

Recent observational constraints on the parameters defined by Eqs. (1.45) and (1.50) have been derived from CMB temperature and polarization anisotropy measurements [9,31]. These are summarized on Table 3, which reveals a nearly scale-invariant scalar power spectrum, as well as an upper bound on the amplitude of the tensor power spectrum. Within the range of scales probed by CMB experiments, these results are consistent with the predictions of a variety of single-field inflation models [32]. The question of whether these measurements can constrain inflationary history in a model-independent way is addressed in Chapter 2.

2.0 INFLATIONARY DYNAMICS RECONSTRUCTION VIA INVERSE-SCATTERING THEORY

The evolution of inflationary fluctuations can be recast as an inverse scattering problem. In this context, we employ the Gel'fand-Levitan method from inverse-scattering theory to reconstruct the evolution of both the inflaton field freeze-out horizon and the Hubble parameter during inflation. We demonstrate this reconstruction procedure numerically for a scenario of slow-roll inflation, as well as for a scenario which temporarily departs from slow-roll. The field freeze-out horizon is reconstructed from the accessible primordial scalar power spectrum alone, while the reconstruction of the Hubble parameter requires additional information from the tensor power spectrum. We briefly discuss the application of this technique to more realistic cases incorporating estimates of the primordial power spectra over limited ranges of scales and with specified uncertainties.

2.1 THE RECONSTRUCTION PROGRAM FOR INFLATION

An early period of accelerated cosmic expansion, referred to as inflation, can successfully account for the observed large-scale properties of our Universe [22, 23]. The inflationary paradigm also provides a natural and appealing mechanism for the generation of density perturbations with the correct statistical properties to seed the growth of structure in the Universe via gravitational instability (see Refs. [33, 34] for a review). However, despite the concordance between observations and the predictions of an inflationary scenario, the physics responsible for driving inflation remains largely speculative.

The reconstruction program for inflation has the goal of probing the physics behind the

inflationary expansion by constraining the process of inflation from observable features of the Universe. The most direct source of information about the inflationary epoch is the primordial power spectrum of density perturbations, $P_{\mathcal{C}}(k)$, and, if eventually detected, of tensor perturbations, $P_T(k)$. The importance of the primordial density perturbations is due to their origin as quantum fluctuations in the "inflaton" field driving inflation, while it is generally thought that quantum fluctuations in the gravitational field during inflation will produce tensor perturbations. The expansion history during inflation is imprinted in both. Measurements of the primordial power spectra over a sufficiently wide range of scales will strongly constrain the possible inflation expansion histories [35] and thus physics at energy scales far higher than are accessible in any conceivable accelerator experiment. Current measurements of the microwave background temperature anisotropies show that the primordial density power spectrum is a power law over an order of magnitude in wave number [34, 36], and the amplitude and slope of the power spectrum already rules out a range of inflation models [34].

Drawing conclusions about inflation dynamics from measurements (or imagined future measurements) has typically been done in one of two ways. The first is with a perturbative expansion around slow-roll inflaton dynamics, which gives constraints on the slow-roll parameters given the amplitude and power-law index of scalar and tensor perturbations at the scale of the horizon today [34]. A measurement of the tensor amplitude at solar-system scales would provide a much longer lever arm and additional slow-roll parameter constraints [37]. The fact that both scalar and tensor perturbations arise from the same inflation dynamics gives consistency relations between the amplitudes and power laws which must be satisfied if inflation dynamics are in the slow-roll regime [38, 39]. While confirmation of these consistency relations would constitute an impressive success of the inflation idea, this type of analysis can reveal inflation dynamics across a relatively limited portion of the inflationary epoch since it is essentially an expansion around the time when perturbations on the scale of the present horizon were generated. Moreover, extending the slow-roll expansion to second order leads to non-perturbative corrections in the reconstructed inflation dynamics [40], indicating lack of convergence in the slow-roll expansion. A second more general technique is to generate inflation models with a large range of expansion histories, then pick out the

ones which are consistent with a given set of perturbation spectra measurements [35, 41]. This technique can incorporate entire inflation histories, but it is difficult to quantify the resulting constraints on inflation because there is no natural prior probability on the space of inflation models [41].

Instead of picking inflation models and seeing if they satisfy some set of measurements, an alternative possibility is to do the reverse: find the constraints on the inflation history which arise directly from the measurements. While calculating power spectra given an inflation model is straightforward, inferring an inflation model given a density power spectrum is more challenging. Habib et al. [42] pointed out that this problem is formally analogous to inverse-scattering theory in quantum mechanics.

The task of inverse-scattering theory is to determine the features of the scattering target, given the distant-past input and far-future scattered output waves. In the context of inflation, the early time evolution of the incoming wave functions are set by the Bunch-Davies vacuum conditions and the late time scattered wave functions are characterized by a freeze-out behavior as they become super-horizon. This formalism identifies the inflaton freeze-out horizon as the effective scattering potential and the primordial power spectrum as the scattering data. The freeze-out horizon can then be used to reconstruct the evolution of the scale factor and Hubble parameter during inflation. This last step requires the amplitude of the tensor power spectrum at a fiducial scale.

A formal solution to the quantum inverse scattering problem was developed by Gel'fand, Levitan, and Marchenko [43–45]. In this paper, we implement a numerical solution to the Gel'fand-Levitan-Marchenko equation in the context of inflation, given exact knowledge of the primordial density power spectrum. We demonstrate the recovery of both a purely slow-roll inflation model and an inflation model with a brief period of fast-roll evolution. This calculation provides the basic groundwork for inferring an inflation model based on partial data about the primordial density power spectrum, possibly combined with measurement of the primordial tensor power spectrum on one or more scales. It has the advantage of relying solely on measurable quantities, making no assumption about the form of the inflaton potential and thus providing model-independent constraints on inflation assuming only the standard connection between perturbation amplitude and scale factor evolution.

In Section 2.2 the evolution of inflationary fluctuations is recast as an inverse-scattering problem and the Gel'fand-Levitan method for the inversion of scattering problems is introduced. Section 2.3 is devoted to a numerical solution of the inverse-scattering problem in the context of inflation, resulting in the reconstruction of the field freeze-out horizon and the Hubble parameter. Finally, in the concluding section we discuss the application of these numerical techniques to more realistic cases incorporating estimates of the primordial power spectra over limited ranges of scales and with specified uncertainties. Some calculation details are summarized in the Appendix. Natural units with $\hbar = c = 1$ are adopted throughout.

2.2 INFLATION AS AN INVERSE-SCATTERING PROBLEM

Following Ref. [42], we rephrase the evolution of inflationary perturbations as a scattering problem and discuss how the Gel'fand-Levitan method from inverse-scattering theory can be used to reconstruct inflation dynamics. First, make the two following substitutions in Eq. (1.40):

$$r = -\eta \quad \text{and} \quad q(-r) = V(r) + \ell\,(\ell+1)\,r^{-2}\,. \tag{2.1}$$

The result resembles a radial time-independent Schrödinger equation for a wave-function $\phi(k, r)$ interacting with a central potential $V(r)$:

$$\phi''(k,\,r) + \left[k^2 - \frac{\ell(\ell+1)}{r^2} - V(r)\right]\phi(k,\,r) = 0\,, \tag{2.2}$$

where ℓ is a constant determined by the form of the primordial power spectrum $P_{\mathcal{C}}(k)$.

From the Bunch-Davies vacuum choice, it also follows that each wave-function behaves as an incoming wave $\phi(k,\,r) \sim \exp\,(ikr)$ for $r \longrightarrow \infty$. In this picture, every mode ϕ_k is now represented by an incident particle of energy k^2 and angular momentum ℓ scattering off of a central potential. The description of inflationary fluctuations as the evolution of modes of different scales has therefore been replaced by the scattering of fictitious particles with varying energies and fixed angular momentum. The mathematical treatment for this class

of scattering problem is well known from inverse-scattering theory.

To apply inverse-scattering techniques, the potential must satisfy the regularity condition

$$\int_b^\infty |V(r)|\, r\, \mathrm{d}r < \infty \quad \text{for} \quad b \geq 0\,. \tag{2.3}$$

This expression imposes that $V(r)$ must decrease faster than r^{-2} as $r \longrightarrow \infty$. This will always hold for single field inflation as long as the expansion is nearly exponential in the deep past. Indeed, in this case it is known that the freeze-out horizon behaves approximately as $q \simeq 2\, r^{-2}$ for large values of r. From (2.1) it then follows that the "centrifugal" term $\ell\,(\ell+1)\, r^{-2}$ retains the relevant functional form in the large r regime, implying that the potential must fall faster than r^{-2} when $r \longrightarrow \infty$. Eq. (2.3) also imposes a degree of regularity on the behavior of $V(r)$ for $r \longrightarrow 0$, but the form of the potential near the origin is not observationally accessible, as it can only be probed by particles (or modes) with extremely large values of k. Thus, $V(r)$ can be assumed to be regular for $r \longrightarrow 0$ without significantly affecting the reconstruction procedure. This will become particularly evident once the Gel'fand-Levitan formalism is stated in the discussion that follows. This shows that a potential $V(r)$ associated with a general single field inflation model can be regarded as regular over the entire range of interest and, consequently, that inverse-scattering tools apply without restrictions in the context of single field inflation.

The task of inverse-scattering theory is to determine the shape of a scattering potential, $V(r)$, from the information contained in the scattered wave-functions. This information is encapsulated in the so-called Jost function, denoted by $F_\ell(k)$, which is constructed from a specific combination of ingoing and outgoing scattering solutions. Habib et. al [42] showed that, in the context of inflation, the Jost function could be related to $P_{\mathcal{C}}(k)$ through the following expression (see Appendix A for more details):

$$|F_\ell(k)|^2 = \frac{r_0^2 \pi^2}{8G\left|\Gamma\left(\ell+\frac{1}{2}\right)\right|^2}\left(\frac{k}{2}\right)^{2\ell-2} P_{\mathcal{C}}(k)\,, \tag{2.4}$$

where both r_0 and ℓ are constants of the scattering problem determined by the primordial power spectrum $P_{\mathcal{C}}(k)$. The Jost function also satisfies the following asymptotic condition: $\lim_{k\to\infty}|F_\ell(k)| = 1$ (see Refs. [46–49] for detailed treatments).

This method provides a solution to the Gel'fand-Levitan-Marchenko equation

$$K(r,\, s) + G(r,\, s) + \int_0^r K(r,\, t)\, G(t,\, s)\, \mathrm{d}t = 0\,, \tag{2.5}$$

which relates the input kernel

$$G(r,\, s) = \frac{2}{\pi} \int_0^\infty S_\ell(rk)\, S_\ell(sk) \left[|F_\ell(k)|^{-2} - 1 \right] \mathrm{d}k \tag{2.6}$$

to the output kernel $K(r, s)$. Here $S_\ell(x)$ are the Ricatti-Bessel functions defined in terms of the usual spherical Bessel functions as $S_\ell(x) = x j_\ell(x)$. Equation (2.5) is a Fredholm integral equation of the second kind which can be solved for $K(r, s)$ by a separable-kernel decomposition, as explained in Appendix B. Once $K(r, s)$ is obtained, the scattering potential is given by

$$V(r) = 2 \frac{d}{dr} K(r,\, r)\,. \tag{2.7}$$

The scattering potential determines directly the inflation freeze-out horizon $q(\eta)$ by Eq. (2.1).

Once $q(\eta)$ is determined, the Mukhanov variable is the solution to

$$z'' = q(\eta)\, z \tag{2.8}$$

and the scale factor satisfies

$$a'' = 2\, \frac{a'^2}{a} - \frac{z(\eta)^2}{2} \frac{a'^2}{a^3}\,, \tag{2.9}$$

which follow from the definitions of $q(\eta)$ and $z(\eta)$. It is convenient to change the independent variable in these differential equations to $\ln(-\eta)$ in order to facilitate their numerical treatment.

The solutions for both (2.8) and (2.9) require initial conditions for $z(\eta)$ and $a(\eta)$. It can be shown, however, that the two initial conditions follow from the amplitude of the tensor power spectrum at CMB scales, where the inflaton field is expected to be slow-rolling and the primordial tensor power spectrum has the form $P_T \propto H^2$. Once these initial conditions are determined, the above equations can be integrated as an initial value problem.

To obtain the initial conditions for $z(\eta)$ and $a(\eta)$ from $P_T(k)$ and the slow-roll conditions, note that at CMB scales the freeze-out horizon is $q = (2 + 3\epsilon)/r^2$ to first order in slow-roll parameters. Since the potential $V(r)$ represents deviations from exactly exponential inflation

it must be small at CMB scales, and the freeze-out horizon is dominated by the centrifugal term in Eq. (2.1), $q = \ell\,(\ell+1)/r^2$. Therefore, to lowest order in slow-roll $\ell \approx 1+\epsilon$ or, equivalently, $\ell \approx (3-n_s)/2$ in terms of the spectral index, n_s. Furthermore, the Mukhanov variable at such scales is $z = r_0/r^\ell$, where r_0 is obtained from the power spectrum normalization at a fiducial CMB scale, k_0. This can be done by evolving the mode of wavenumber k_0 from the distant past through freeze-out and computing $P_{\mathcal{C}}(k_0)$ for different values of r_0. Matching this value with the known power spectrum normalization at k_0 singles out a value for r_0. Since $P_{\mathcal{C}}(k)$ is known at CMB scales, the constants ℓ and r_0 can be determined from the power spectrum slope and normalization, respectively. Alternatively, one could also determine the value of r_0 from the small k expansion of the Jost function derived in [42]. Therefore, the initial conditions z and z' for Eq. (2.8) can be computed from $z = r_0/r^\ell$, where the initial value of r is given by the horizon crossing relation $k(r) = \sqrt{q(r)}$. The initial conditions a and a' for Eq. (2.9) then follow from the slow-roll condition $z' \simeq (a'/a)z$, the definition of the Hubble parameter $H = a'/a^2$, and a measurement of $P_T \propto H^2$ at CMB scales.

Thus, the necessary initial condition for reconstructing the Mukhanov variable and the scale factor during inflation, and by consequence the Hubble parameter, can be obtained from a measurement of the amplitude of the primordial tensor power spectrum at CMB scales.

2.3 ANALYSIS AND RESULTS

Numerical solutions to Eq. (2.5) provide information about arbitrary inflation dynamics; an assumption of slow-roll behavior only comes in to initial conditions at CMB scales, where observations of $P_{\mathcal{C}}(k)$ show this is likely a good assumption [34]. We demonstrate numerical solutions in two particular cases, corresponding to single-field inflation models with the scalar potentials

$$V_A(\Phi) = m^2\Phi^2\,, \tag{2.10a}$$

$$V_B(\Phi) = m^2\Phi^2\left[1 + c\tanh\left(\frac{\Phi - \Phi_s}{d}\right)\right]. \tag{2.10b}$$

While the first potential has the standard quadratic form and corresponds to a model in which the inflaton field is slow-rolling for most of its evolution, the second potential possesses the interesting characteristic of allowing the inflaton field to temporarily deviate from slow-roll when $\Phi \approx \Phi_s$. The constants c and d correspond to the amplitude and breadth of a small step in the potential, which is responsible for the departure from slow roll. These potentials are shown in Figure 3 and their resulting scalar power spectra $P_{\mathcal{C}}(k)$ in Figures 4 and 5. The primordial power spectra were numerically generated according to the standard mode freeze-out formalism reviewed in Section 1.5 (see [50] for a detailed description of the numerical aspects of this calculation).

For a rigorous application of the Gel'fand-Levitan method we should have access to $P_{\mathcal{C}}(k)$ for all k. However, in practice our knowledge is limited by the range of scales accessible to our experiments. Here we study three scenarios in which we assume access to $P_{\mathcal{C}}(k)$ up to $k_\star = 10^4$, 10^6, and $10^8\,\mathrm{Mpc}^{-1}$. Our choices of cut-off scales span the range over which future information on the primordial power spectrum may be available from various sources including strong lensing [51], dynamics of tidal streams [52], and microwave background spectral distortions [53]. Furthermore, from the asymptotic behavior of the Jost function we notice that any information contained in the spectrum of extremely small scales should not contribute significantly to the reconstruction procedure. This is clearly seen from the integrand of Eq. (2.6) which tends to zero for large values of k.

A simple toy model which illustrates the procedure discussed in Section 2.2 is the trivial case of inflation driven by a constant inflaton potential resulting in eternal exponential expansion. In this case the primordial power spectrum is exactly scale invariant $P_{\mathcal{C}}(k) \propto k^0$, and the slow-roll parameter vanishes $\epsilon = 0$. Therefore, following our previous discussion, $\ell = 1$. As a result the Jost function, Eq. (2.4), will also be scale invariant $|F_\ell(k)|^2 \propto r_0^2$, where a suitable value for r_0 can always be found. A constant Jost function implies that both input and output kernels are identically zero, $G(r,\, s) = K(r,\, s) = 0$. As a consequence, the scattering potential given by Eq. (2.7) is $V(r) = 0$. Finally, from Eq. (2.1) the frezee-out horizon is found to be $q = 2\,r^{-2}$ which is in agreement with the theoretical result for de

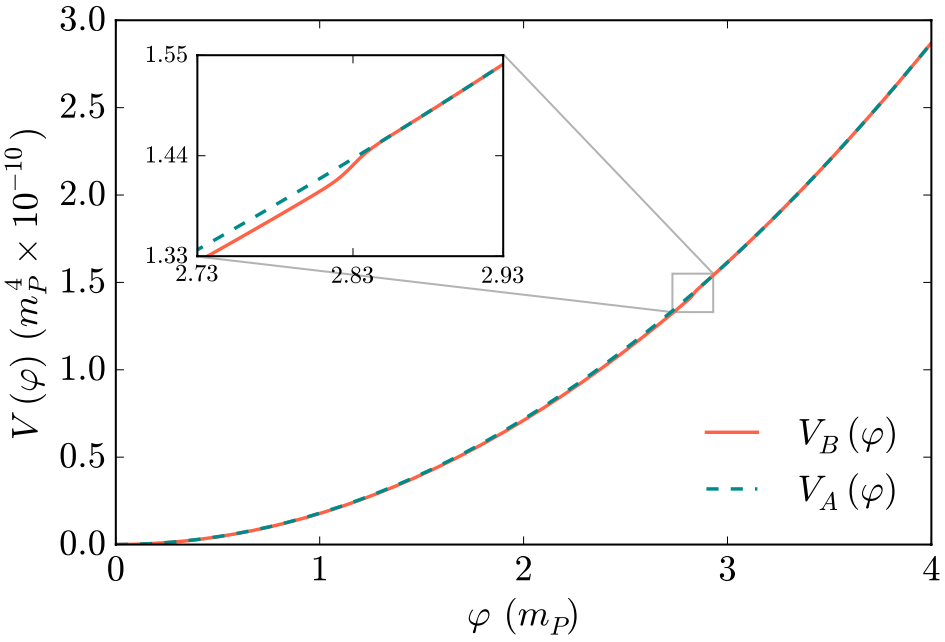

Figure 3: Plot of the inflaton potentials used to obtain the simulated primordial power spectra. The dashed line shows the quadratic potential, $V_A(\Phi)$, while the solid line corresponds to the potential $V_B(\Phi)$.

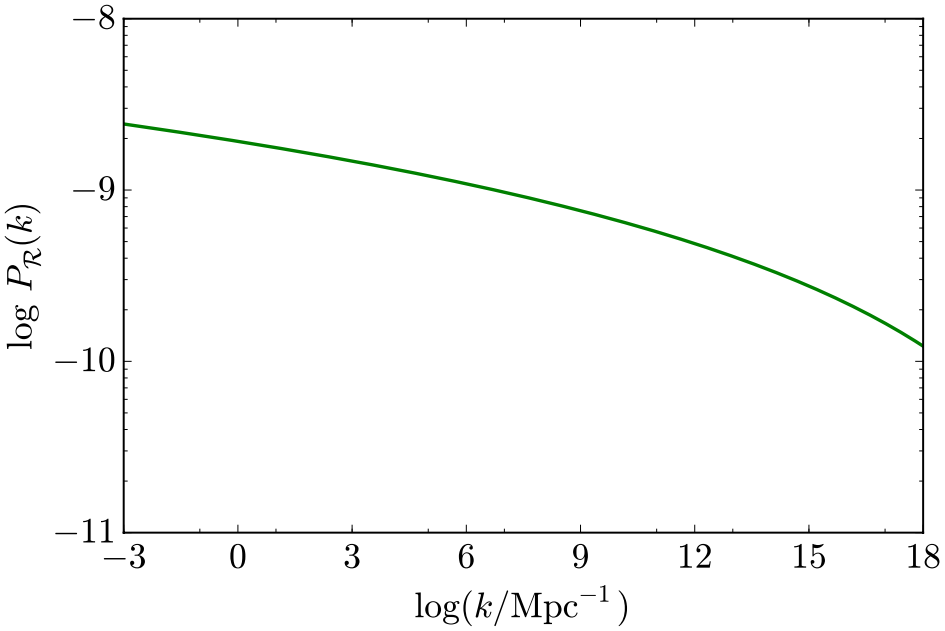

Figure 4: Primordial power spectra associated with the potential $V_A(\Phi)$. The curve is normalized according to Planck results at the pivot scale $k_0 = 0.05\,\mathrm{Mpc}^{-1}$, such that $P_{\mathcal{C}}(k_0) = 2.196 \times 10^{-9}$.

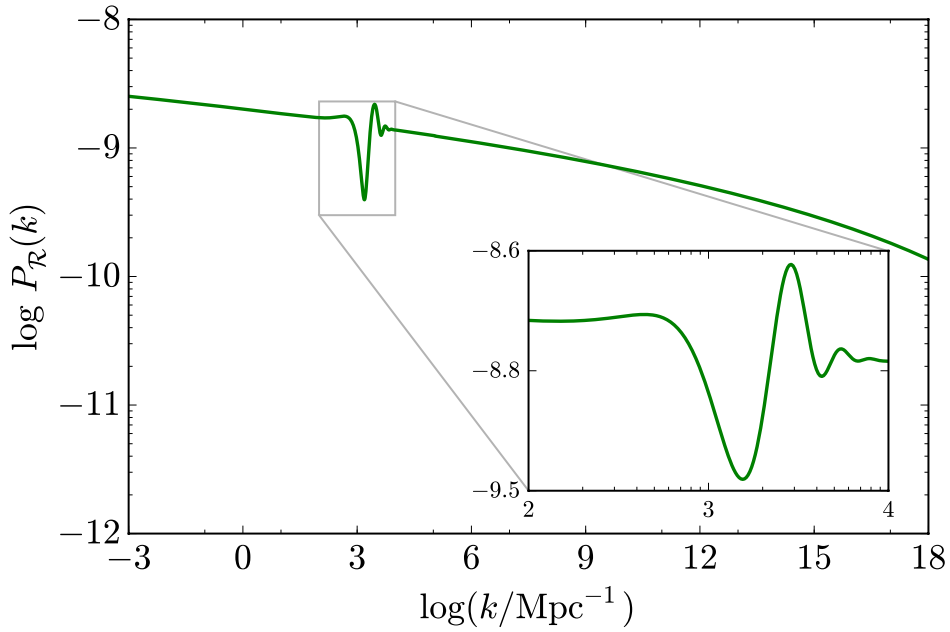

Figure 5: Primordial power spectra associated with the potential $V_B(\Phi)$. The inset focuses on the ringing feature generated by the potential step. The curve is normalized according to Planck results at the pivot scale $k_0 = 0.05\,\mathrm{Mpc}^{-1}$, such that $P_{\mathcal{C}}(k_0) = 2.196 \times 10^{-9}$.

Sitter space.

The procedure is analogous for the more complicated inflationary potentials of Eqs. (2.10a) and (2.10b). The values of ℓ and r_0 are determined from the scalar power spectrum slope and normalization, respectively. For the cases studied in this work we obtained $\ell = 1.008$ since $\epsilon = 0.008$ when CMB scales exit the horizon in our simulations. The value of r_0 follows from the normalization at the pivot scale $k_0 = 0.05\,\mathrm{Mpc}^{-1}$, such that $P_{\mathcal{C}}(k_0) = 2.196 \times 10^{-9}$.

The numerical value of the input kernel is found by evaluating the highly oscillatory integral in Eq. (2.6) up to $k_\star$. In this work this computation was performed using the Levin collocation method of integration [54] (see Appendix C) which takes into account the fact that the Jost function is, in the most general scenario, a non-smooth function of k. The parameters r and s both range over the interval $(0,\, k_\star)$. The expression for the input kernel is closely related to the two dimensional Fourier transform [45] of the scattering function in radial coordinates, which is commonly used in inverse-scattering theory.

The reconstruction procedure is then carried out by employing the inverse-scattering formalism. The output kernel follows as a solution of the Gel'fand-Levitan-Marchenko equation, which can be rewritten as a set of linear equations assuming the input kernel is separable,

$$G(r,\, s) = \sum_i a_i(r)\, b_i(s)\,. \tag{2.11}$$

A detailed derivation is presented in Appendix B. The reconstructed freeze-out horizon obtained from this analysis for both model potentials in Eqs. (2.10a) and (2.10b) are shown in Figures 6 and 7 for the cut-off scales $k_\star = 10^4$, 10^6, and $10^8\,\mathrm{Mpc}^{-1}$. Along with these physically well-motivated choices of $k_\star$ we also plot the reconstructed curve obtained with $k_\star = 10^{18}\,\mathrm{Mpc}^{-1}$ as a mere demonstration of numerical convergence of the reconstruction procedure with increasing cut-off scales.

Figure 6 shows that in the case of a featureless power spectrum, choosing a cut-off scale of $k_\star = 10^4\,\mathrm{Mpc}^{-1}$ preserves the overall functional form of the reconstruction, but induces an average relative error which is approximately 2 % larger compared to that obtained for $k_\star = 10^8\,\mathrm{Mpc}^{-1}$. We obtained average errors of 9.7 %, 8.8 %, and 7.6 % for $k_\star = 10^4$, 10^6, and $10^8\,\mathrm{Mpc}^{-1}$, respectively.

On the other hand, if the primordial power spectrum possesses features such as the ring-

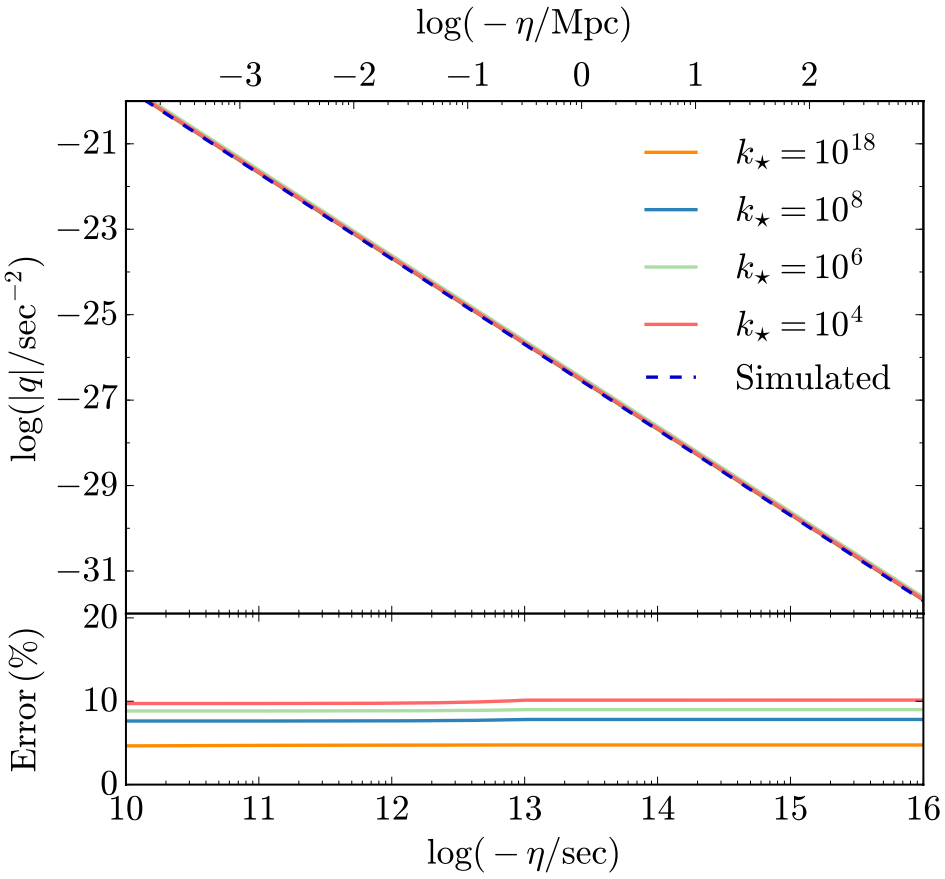

Figure 6: Reconstruction of the freeze-out horizon of $V_A(\Phi)$ for different choices of the cut-off scale, $k_\star$ (in units of Mpc^{-1}). The larger the value of $k_\star$ the better the reconstruction, as shown in the lower panel by the difference between the simulated and the reconstructed curves. The case with cut-off $k_\star = 10^{18}\,\mathrm{Mpc}^{-1}$, although not physically well-motivated, is shown to demonstrate the convergence of the reconstruction procedure.

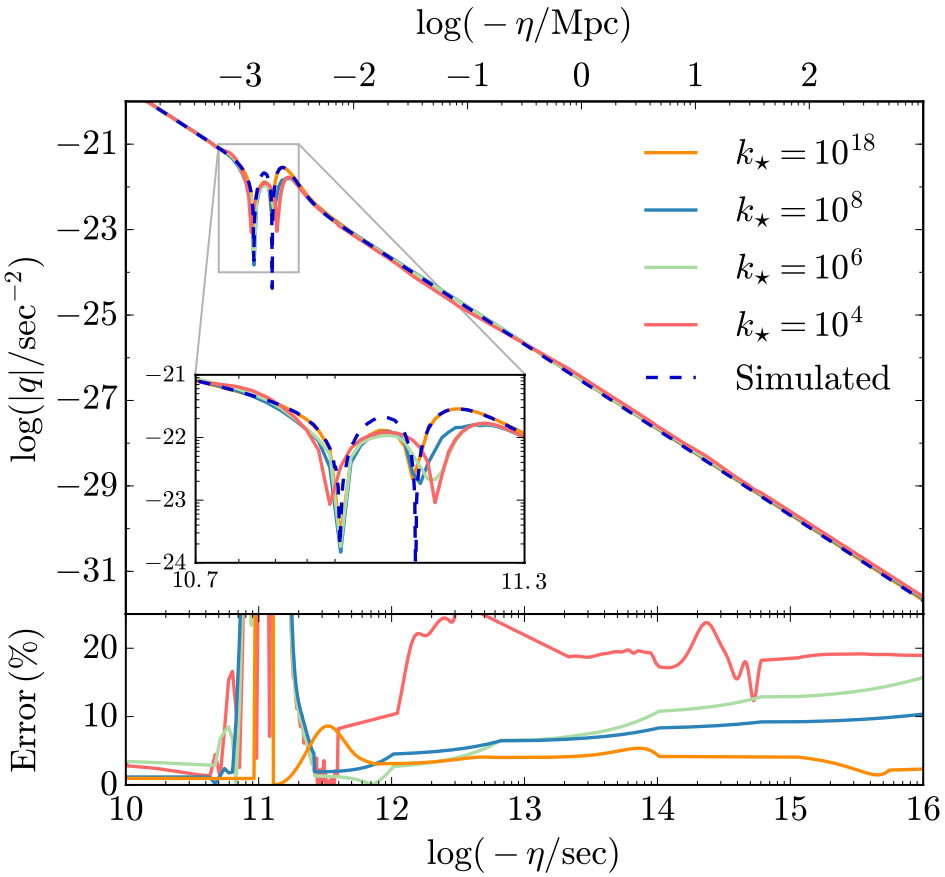

Figure 7: Reconstruction of the freeze-out horizon of $V_B(\Phi)$ for different choices of the cut-off scale, $k_\star$ (in units of Mpc^{-1}). For the regions where the primordial power spectrum is featureless the reconstruction of $q(\eta)$ resembles the simulated curve. However, whenever features are present, the corresponding features in the reconstructed $q(\eta)$ are suppressed. The larger the value of $k_\star$ the better the reconstruction, as can be clearly seen in this case. The case with cut-off $k_\star = 10^{18}\,\mathrm{Mpc}^{-1}$, although not physically well-motivated, is shown to demonstrate the convergence of the reconstruction procedure. The inset shows a close-up of the feature. The difference between the simulated and the reconstructed curves is shown in the lower panel.

ing oscillations shown in Figure 5, the corresponding feature in the reconstructed freeze-out horizon is suppressed and broadened for small cut-off scales. This can be seen in Figure 7. The quality of our results for this case depends on whether the reconstructed region contains the feature. The average error in the region which does not contain the feature is of 6.7 % for our largest choice of cut-off scale $k_\star = 10^8\,\mathrm{Mpc}^{-1}$, while for $k_\star = 10^6$ and $10^8\,\mathrm{Mpc}^{-1}$ the average errors are of 7.2 %, and 11.4 %, respectively. These errors, although dependent on the choice of cut-off, are expected to decrease with higher numerical resolution. The region containing the feature is harder to reconstruct and represents a difficult numerical challenge. In this region, the average percentage difference between the simulated and reconstructed curves for $k_\star = 10^8\,\mathrm{Mpc}^{-1}$ is of 48 %. Bringing the cut-off scale down to $k_\star = 10^6$ and $10^4\,\mathrm{Mpc}^{-1}$ increases the average relative error to 72% and 75%, respectively. However, the characteristic shape of the feature is reproduced successfully.

The inverse-scattering formalism shows that we can recover the freeze-out horizon, $q(\eta)$, from the scalar power spectrum alone. To reconstruct the expansion history, however, additional information is needed for the integration of Eqs. (2.8) and (2.9). In principle, as explained in Section 2.2, the amplitude of $P_T(k)$ at CMB scales could provide the necessary initial conditions for the numerical solution of these equations, allowing us to reconstruct $a(\eta)$ and $z(\eta)$. We have reconstructed H from the freeze-out horizon assuming that the amplitude of the primordial tensor power spectrum is known at $k_0 = 0.05\,\mathrm{Mpc}^{-1}$. The numerical errors in the reconstructed freeze-out horizon make the initial step in the integration of Eq. (2.8) inconsistent with the initial conditions derived for the Mukhanov variable at CMB scales. In order to eliminate this inconsistency we rescale the reconstructed freeze-out horizon by a constant factor to ensure it agrees with its known slow-roll value at CMB scales, $q = \ell\,(\ell+1)\,\eta^{-2}$. This operation preserves the overall shape of the freeze-out horizon and also guarantees consistency in the integration of Eq. (2.9).

Figures 8 and 9 show the reconstructed and simulated Hubble parameters for our choices of inflationary models expressed as a function of the number of e-folds, N. As expected, the reconstructed Hubble parameter is significantly more accurate close to $N \approx 60$, as the procedure relied on initial conditions extracted at CMB scales. The agreement between expected and reconstructed curves is markedly better for the model with a featureless quadratic po-

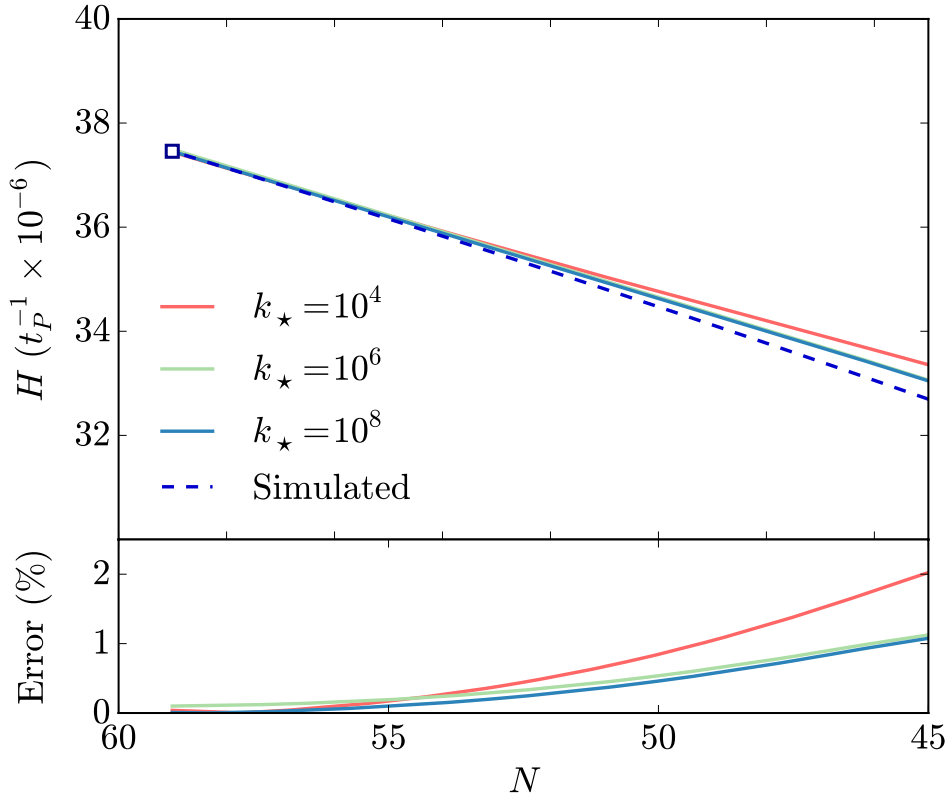

Figure 8: Hubble parameter associated with the potential $V_A(\Phi)$ for different choices of the cut-off scale, $k_\star$ (in units of Mpc^{-1}). The upper panel shows the simulated (dashed lines) and the reconstructed (solid lines) curves for the Hubble parameter, H (in units of the inverse Planck time), as a function of the number of e-folds, N. The relative error between these curves is shown in the lower panel. These reconstructions assume knowledge of the amplitude of $P_T(k)$ at $k_0 = 0.05\,\mathrm{Mpc}^{-1}$ (represented on the plots by a square marker at $N \approx 60$).

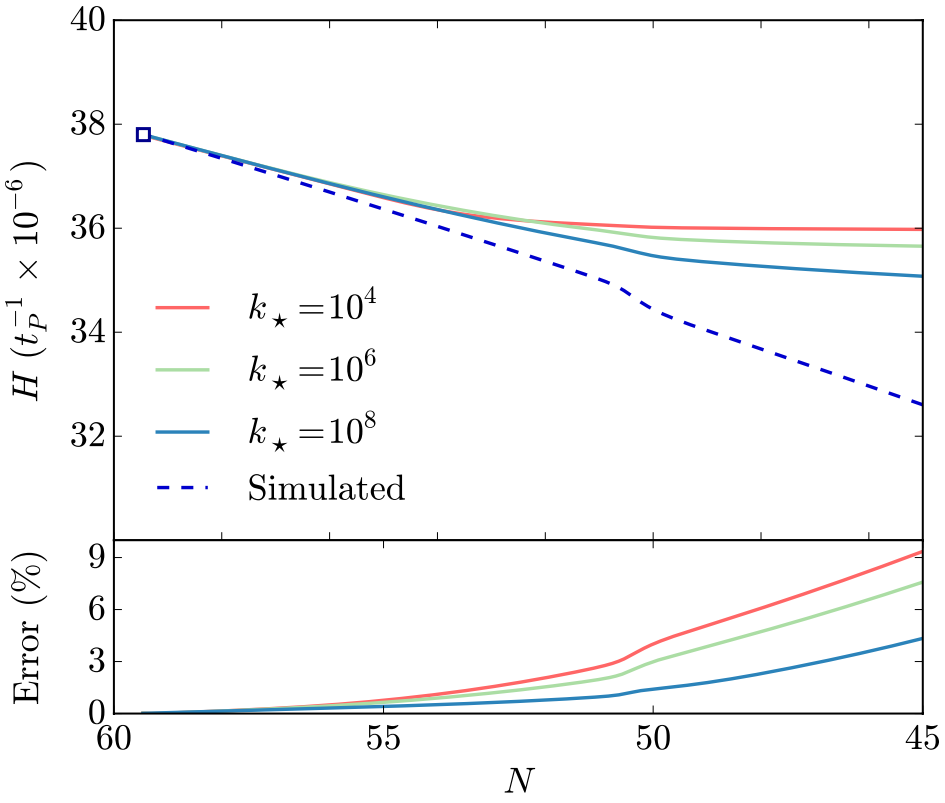

Figure 9: Hubble parameter associated with the potential $V_B(\Phi)$ for different choices of the cut-off scale, $k_\star$ (in units of Mpc^{-1}). The upper panel shows the simulated (dashed lines) and the reconstructed (solid lines) curves for the Hubble parameter, H (in units of the inverse Planck time), as a function of the number of e-folds, N. The relative error between these curves is shown in the lower panel. These reconstructions assume knowledge of the amplitude of $P_T(k)$ at $k_0 = 0.05\,\mathrm{Mpc}^{-1}$ (represented on the plots by a square marker at $N \approx 60$).

tential and a choice of large cut-off scale. As for the potential with a step, the errors in the reconstructed $q(\eta)$ significantly affect the computation of $a(\eta)$, and consequently of H. In this case the reconstruction could benefit from improved $q(\eta)$ curves computed with higher numerical resolution, although the errors associated to the region containing the feature would still be large enough to affect the reconstruction for $N < 50$. Nevertheless, even though in this case the reconstructed curve may deviate significantly from the simulated solution, it is still possible to identify in Figure 9 the presence of a step in the evolution of H at $N \approx 50$ for $k_\star = 10^8\,\mathrm{Mpc}^{-1}$.

2.4 FUTURE PROSPECTS

A formal analogy between determining inflationary dynamics from metric perturbations and determining a spherically symmetric quantum scattering potential from scattering data has been known for some time. We have obtained a numerical reconstruction of inflation dynamics given a known scalar perturbation power spectrum via the Gel'fand-Levitan method: First, take a primordial scalar power spectrum as input data and from it compute the Jost function. Second, numerically evaluate a highly oscillatory intergral to obtain the input kernel. Third, convert the Gel'fand-Levitan-Marchenko equation into a system of linear equations to obtain the freeze-out horizon as a function of scale from the derivative of the output kernel. Fourth, solve a set of differential equations to obtain the evolution of the Hubble parameter during inflation from the freeze-out horizon assuming we know the amplitude of the primordial tensor power spectrum. We performed these calculations for both a standard slow-roll inflation model and a model with an inflaton potential step resulting in a period of fast-roll dynamics, obtaining reasonably good agreement between simulated and reconstructed freeze-out horizon (Figures 6 and 7) and Hubble parameter (Figures 8 and 9). We have thus demonstrated that numerical computation of arbitrary inflation dynamics using the Gel'fand-Levitan method can be numerically stable and accurate over the wide range of scales for which inflation observables can potentially be observed. We use the assumption that the potential was slow-rolling in the infinite past in order to establish the value of ℓ

when solving for the freeze-out horizon.

This calculation can form the basic building block for model-independent estimation of inflation dynamics from noisy measurements of the primordial density power spectrum. For a given set of power spectrum measurements and covariances, the most likely inflation dynamics is a well-posed Bayesian inference problem, since a calculation like the one here maps any given power spectrum into a particular inflation history. An additional possible future source of information is the power spectrum of tensor perturbations produced during inflation; the amplitude of a tensor spectrum depends on the energy scale at which inflation occurred. If large enough to be detected at one or more length scales, the tensor perturbations will provide additional constraints which can be folded into the model inference or incorporated as priors on the inflation effective potential obtained from the scalar perturbations. For instance, the measurement of tensor modes at both CMB and Solar System scales could be used as boundary conditions for the inference of inflationary history at intermediate scales which are beyond the reach of current and future experiments. Inflation dynamics estimation from noisy and incomplete power spectrum data will be considered elsewhere.

The basic technique of inverting observations to get estimates of the inflation dynamics is opposite to the forward modeling which is generally used to constrain inflation: given an inflation model, its predicted perturbation power spectra can be computed in a straightforward manner, and then compared to data. Many inflation models can be ruled out this way. But it is difficult to quantify which inflation model is most likely, because any parameterization of the space of models has no natural measure for prior probability.

The wider the range of length scales covered by power spectrum measurements, the longer the period of inflationary dynamics that can be recovered. Current cosmic microwave background experiments, large-scale structure surveys, and Lyman-alpha observations give a reasonably precise measurement of the primordial power spectrum for wave numbers between $0.01\,\mathrm{Mpc}^{-1} < k < 1\,\mathrm{Mpc}^{-1}$ [34, 36, 55–59]. Microwave background spectrum distortions in principle contain information about perturbations at smaller scales [53]. It is also possible that primordial perturbations on subgalactic scales will eventually be probed by high-sensitivity gravitational lensing, galaxy dynamics measurements or improved understanding of the dwarf galaxy population. Tensor perturbations may be seen at horizon scales in mi-

crowave background B-mode polarization, and if the tensor amplitude is large enough to be detected this way, then ultimately the tensor perturbations may also be measured at a vastly smaller Earth-Sun scale by a space-based laser interferometer [37, 60].

Some of these signals may be beyond the ultimate reach of experiments, but long-term prospects exist for significantly enhanced experimental information about inflation-produced perturbations. Inverting the data to obtain constraints on inflation dynamics will allow us to make the most of these remarkable observational possibilities.

3.0 QUANTUM PARTICLE PRODUCTION EFFECTS ON COSMIC EXPANSION

Quantum fields in cosmological spacetimes can experience particle production due to their interaction with the expanding background. This effect is particularly relevant for models of the very early Universe, when the energy density generated through this process may back-react on the cosmological expansion. Yet, these scenarios have not been fully explored due to the several technical hurdles imposed by the back-reaction calculations. In this work we review the basics of cosmological quantum particle production and demonstrate a numerical algorithm to solve the back-reaction problem in regimes dominated by particle production. As an illustration, we compute the effects of a massive quantized scalar field on a cosmological bounce scenario, explicitly showing that quantum particle production can cause the contracting phase to end in a radiation crunch, or can delay the bounce. Finally, we discuss the relevance of quantum particle production/annihilation to bounce and inflationary models of the early Universe.

3.1 REVIEW OF QUANTUM PARTICLE PRODUCTION AND MOTIVATIONS

In his pioneering 1968 Ph.D. thesis, Leonard Parker discovered the surprising phenomenon that evolving cosmological spacetimes can produce quantum particles [61–63]. This work laid much of the theoretical framework for our current understanding of quantum fields in curved spacetimes (see, e.g., the textbooks [7, 8]). The phenomenon has since been investigated in astrophysical and cosmological contexts, leading to fundamental theoretical results

including the emission of Hawking radiation by blackholes [64–72]. and the generation of primordial fluctuations during inflation [27, 73–78].

Cosmological quantum particle production results from the shifting quantum vacuum state due to spacetime expansion. A given mode of a quantum field can begin in a state with no particles, but at a later time have a non-zero particle number expectation value. Parker showed that while this does not happen for massless conformally-coupled fields, it is generic for massive scalar fields of arbitrary coupling to the spacetime curvature. Typically, the particle production is significant when the particle mass m is of the order of the expansion rate H, or when $m^2 \simeq \dot{H}$. Simple dimensional arguments show that in a Universe with critical density $\rho_c \simeq 3H^2/8\pi G$, quantum particle production can contribute significantly to the energy density of the Universe at early epochs when H is not too far below the Planck scale.

This effect naturally suggests that quantum particle production may have a significant impact on the expansion rate of the Universe at early times. The back-reaction problem consists in understanding how the energy density generated through this process alters the evolution of the background spacetime. This seemingly straightforward calculation is actually subtle due to two technical challenges of quantum fields in curved spacetimes. First, the definition of the quantum vacuum and particle are not formally well defined in time-varying spacetimes. Second, the energy-momentum tensor of a quantized field propagating on a curved background possesses a formally infinite expectation value, and must be regularized to yield physically sensible results. In homogeneous and isotropic spacetimes, both problems can be addressed via the method of adiabatic regularization [79–84], which is particularly useful for numerical computations. The adiabatic notion of particle offers a clear way to track particle number in a spacetime which is expanding sufficiently slowly. This representation has the special property of defining a vacuum state which comes closest to the Minkowski vacuum when the background expansion is sufficiently slow. However, adiabatic regularization introduces several technical complications to the back-reaction problem. As a consequence, ambiguities arise in specifying initial conditions, and computationally the problem becomes very complicated with potential numerical instabilities [85–89]. In practice, the ambiguities and complexities together have prevented any general numerical

solution, although the test-field limit in which back-reaction effects are neglected has been investigated in several studies [90–94].

Formal developments clarified aspects of the adiabatic regularization approach, offering a clear separation between the energy density due to the field particle content and the divergent contributions from the zero-point energy [94–97]. However, the notion of adiabatic particle appearing in the energy density suffers from ambiguities. For a typical mode of a quantum field, its associated particle number during times of significant particle production depends on the perturbative order of adiabatic regularization employed. This is obviously an unphysical result, since the dominant term in the energy density is often just a simple function of the particle number density. Typically, successive orders of adiabatic regularization gives the particle number in a given mode as a divergent asymptotic series. Recent important papers by Dabrowski and Dunne [98, 99] employed a remarkable result of asymptotic analysis [100–104] to sum the divergent series and provide a sensible notion of particle which is valid at all times. Since any remaining physical ambiguity is then removed from the problem, this result points the way to a general numerical solution.

We combine these recent results into an approach which numerically solves the quantum back-reaction problem in regimes with field energy density dominated by particle production. We then apply this technique to a toy cosmological model, that of a positive-curvature spacetime with a constant energy density (the closed de Sitter model). In the absence of any quantum fields or other particle content, this spacetime exhibits a bounce behavior, contracting to a minimum scale factor and then expanding again. Here we show explicitly that the existence of a massive scalar field in a particular mass range will cause large changes in the spacetime evolution: even if the contracting spacetime initially contains a quantum field in its adiabatic vacuum state, quantum particle production can create enough energy density to push the spacetime into a radiation crunch. Special values of the field mass can also delay but not eliminate the bounce. This appears to be the first general solution for the quantum back-reaction problem in cosmology.

In Section 3.2 we discuss the adiabatic field representation and the semi-classical notion of adiabatic particle number. Section 3.3 recasts quantum particle production in terms of the Stokes phenomenon of the complex-plane wave equation for specific modes, including

interference between different modes. Section 3.4 formulates the back-reaction problem for scenarios in which the field particle content or particle production dominates the field energy density. Section 3.5 outlines our numerical implementation of the mathematical results in Sections 3.3 and 3.4. Physical results for a closed de Sitter model are presented in Section 3.6. Finally, in Section 3.7 we discuss the prospects for more general situations, including quantum fields with spin and interacting quantum fields, and the possible relevance of quantum particle production to early-Universe models, including inflationary and bounce scenarios. Salient technical details are summarized in the Appendix. Natural units with $\hbar = c = 1$ are adopted throughout.

3.2 ADIABATIC REPRESENTATION

Despite the multitude of available representations for a quantized scalar field defined on a FLRW spacetime, one particular choice referred to as the adiabatic representation stands out. This representation has the special property of defining a vacuum state which comes closest to the Minkowski vacuum when the background expansion is sufficiently slow. As a consequence, the adiabatic representation provides the most meaningful notion of physical particle in an expanding homogeneous and isotropic Universe. Here we discuss this representation closely following Ref. [94].

The adiabatic representation is characterized by mode functions which are the phase-integral solutions [61–63] of Eq. (1.28):

$$h_k(t) = \frac{1}{\sqrt{2W_k(t)}} \exp\left(- i \int^t W_k(s)\, \mathrm{d}s \right) , \tag{3.1}$$

where the integral in the exponent can be computed from any convenient reference time, and the function $W_k(t)$ is given by the formal asymptotic series

$$W_k(t) \equiv \Omega_k(t) \sum_{n=0}^{\infty} \psi_{k,\,2n}(t) \, . \tag{3.2}$$

The terms $\psi_{k,\,2n}(t)$ are obtained by substituting Eqs. (3.2) and (3.1) into Eq. (1.28). The expressions which ensue from these substitutions are standard results of the phase-integral method [105, 106]; up to fourth order they are

$$\psi_{k,\,0}(t) = 1\,, \tag{3.3a}$$

$$\psi_{k,\,2}(t) = \frac{1}{2}\varepsilon_{k,\,0}(t)\,, \tag{3.3b}$$

$$\psi_{k,\,4}(t) = -\frac{1}{8}\Big[\varepsilon^{2}_{k,\,0}(t) + \varepsilon_{k,\,2}(t)\Big]\,, \tag{3.3c}$$

for which the quantities appearing on the right-hand sides are given by

$$\varepsilon_{k,\,0}(t) \equiv \Omega_{k}^{-3/2}(t)\,\frac{d^{2}}{dt^{2}}\Big[\Omega_{k}^{-1/2}(t)\Big]\,, \tag{3.4a}$$

$$\varepsilon_{k,\,m}(t) \equiv \left[\Omega_{k}^{-1}(t)\,\frac{d}{dt}\right]^{m}\varepsilon_{k,\,0}(t)\,. \tag{3.4b}$$

In a sense, the functions $W_{k}(t)$ capture the overall time dependence of each $\mathbf{k}$-mode due the evolving FLRW metric, leaving behind only the Minkowski-like mode oscillations which take place on top of this background [98, 99]. It is this property that makes the adiabatic mode functions $h_{k}(t)$ and $h^{*}_{k}(t)$ such good templates for probing the particle content of fields evolving in cosmological spacetimes. This template role is made precise by the following time-dependent generalization of Eqs. (1.34) [61–63], which expresses the field modes $f_{k}(t)$ as linear combinations of the adiabatic mode functions:

$$f_{k}(t) = \alpha_{k}(t)h_{k}(t) + \beta_{k}(t)h^{*}_{k}(t)\,, \tag{3.5}$$

where the Bogolyubov coefficients $\alpha_{k}(t)$ and $\beta_{k}(t)$ are analogous to those appearing in Eqs. (1.34) and (1.35), but are here regarded as time-dependent quantities due to the fact that $h_{k}(t)$ and $h^{*}_{k}(t)$ are merely approximate solutions of Eq. (1.28). In order to completely specify these coefficient functions, an additional expression must be provided. For that purpose, it is common to introduce a condition on the time derivative of the mode function which preserves the Wronskian relation of Eq. (1.31). In its most general form, this condition can

be stated as [94]

$$\dot{f}_k(t) = \left[-iW_k(t) + \frac{V_k(t)}{2} \right] \alpha_k(t) h_k(t) + \left[iW_k(t) + \frac{V_k(t)}{2} \right] \beta_k(t) h_k^*(t) \,. \tag{3.6}$$

Here the arbitrary function $V_k(t)$ contains the residual freedom in the definition of the adiabatic vacuum. In this work we will choose this function to be

$$V_k(t) = -\frac{\dot{W}_k(t)}{W_k(t)} \,, \tag{3.7}$$

as this choice leads to important simplifications in the back-reaction problem.

Gathering Eqs. (1.25) and (3.5), we find that the ladder operators associated with the adiabatic representation satisfy the transformations

$$a_{\mathbf{k}} = \alpha_k^*(t) b_{\mathbf{k}}(t) - \beta_k^*(t) b_{\mathbf{k}}^\dagger(t) \,, \tag{3.8a}$$

$$a_{\mathbf{k}}^\dagger = \alpha_k(t) b_{\mathbf{k}}^\dagger(t) - \beta_k(t) b_{\mathbf{k}}(t) \,, \tag{3.8b}$$

which in turn imply a time-dependent version of Eq. (1.36),

$$\left|\alpha_k(t)\right|^2 - \left|\beta_k(t)\right|^2 = 1 \,. \tag{3.9}$$

Finally, it is useful to characterize field states according to the values of the non-trivial adiabatic bilinears $\langle b_{\mathbf{k}}^\dagger(t) b_{\mathbf{k}}(t) \rangle$ and $\langle b_{\mathbf{k}}(t) b_{\mathbf{k}}(t) \rangle$. The first of these bilinears tracks the adiabatic particle content per comoving volume in the $\mathbf{k}$-mode under consideration. Using the transformations established above by Eqs. (3.8), it follows that

$$\begin{aligned} \mathcal{N}_k(t) &= \langle b_{\mathbf{k}}^\dagger(t) b_{\mathbf{k}}(t) \rangle \\ &= \left|\alpha_k(t)\right|^2 \langle a_{\mathbf{k}}^\dagger a_{\mathbf{k}} \rangle + \left|\beta_k(t)\right|^2 \langle a_{\mathbf{k}} a_{\mathbf{k}}^\dagger \rangle \\ &= N_k + \sigma_k \left|\beta_k(t)\right|^2 , \end{aligned} \tag{3.10}$$

where $N_k = \langle a_{\mathbf{k}}^\dagger a_{\mathbf{k}} \rangle$ is a constant of motion which can be understood as the initial number of adiabatic particles per comoving volume populating the field mode of wavenumber k, and $\sigma_k = 1 + 2N_k$ is the Bose-Einstein parameter responsible for stimulated particle production.

The second bilinear can be expressed as

$$\begin{aligned}\mathcal{M}_k(t) &= \big\langle b_{\mathbf{k}}(t) b_{\mathbf{k}}(t) \big\rangle \\ &= \alpha_k(t)\beta_k^*(t)\big\langle a_{\mathbf{k}}^\dagger a_{\mathbf{k}} \big\rangle + \alpha_k(t)\beta_k^*(t)\big\langle a_{\mathbf{k}} a_{\mathbf{k}}^\dagger \big\rangle \\ &= \sigma_k\, \alpha_k(t)\beta_k^*(t)\,.\end{aligned} \tag{3.11}$$

In principle, these bilinears contain all the required information to track the field evolution and, consequently, the time dependence of the field energy density and pressure. In practice, however, these quantities suffer from an irreducible ambiguity which is particularly pronounced when $\mathcal{N}_k(t)$ and $\mathcal{M}_k(t)$ incur rapid changes, such as when particle production occurs. The root of this issue can be traced back to the asymptotic representation of $W_k(t)$, which is usually handled by simply truncating the series in Eq. (3.2) at a finite order. However, the values of the bilinears depend strongly on where the series is truncated if they are rapidly changing (see Ref. [98] for striking graphical representations). In the next Section, we discuss a technique for finding the exact universal evolution for both adiabatic bilinears which the asymptotic series represents.

3.3 PARTICLE PRODUCTION AND THE STOKES PHENOMENON

The adiabatic representation introduced in the previous section provides an accurate description of the bilinears $\mathcal{N}_k(t)$ and $\mathcal{M}_k(t)$ whenever $|\varepsilon_{k,0}| \ll 1$. The more severely this condition is violated, the more unreliable these adiabatic quantities become. Adiabatic particle production, for instance, coincides with the momentary violation of this condition, implying that the notion of particle remains uncertain until particle production ceases. Nonetheless, a universal notion of particle can be restored for all times when particle production events are understood in terms of the Stokes phenomenon.

The sharp transitions between asymptotic solutions of a given differential equation which are valid in different regions of the complex plane are termed the Stokes phenomenon. These regions are bounded by the so-called Stokes and anti-Stokes lines. In the context of a scalar field evolving in a FLRW spacetime, the differential equation of interest is the equation of

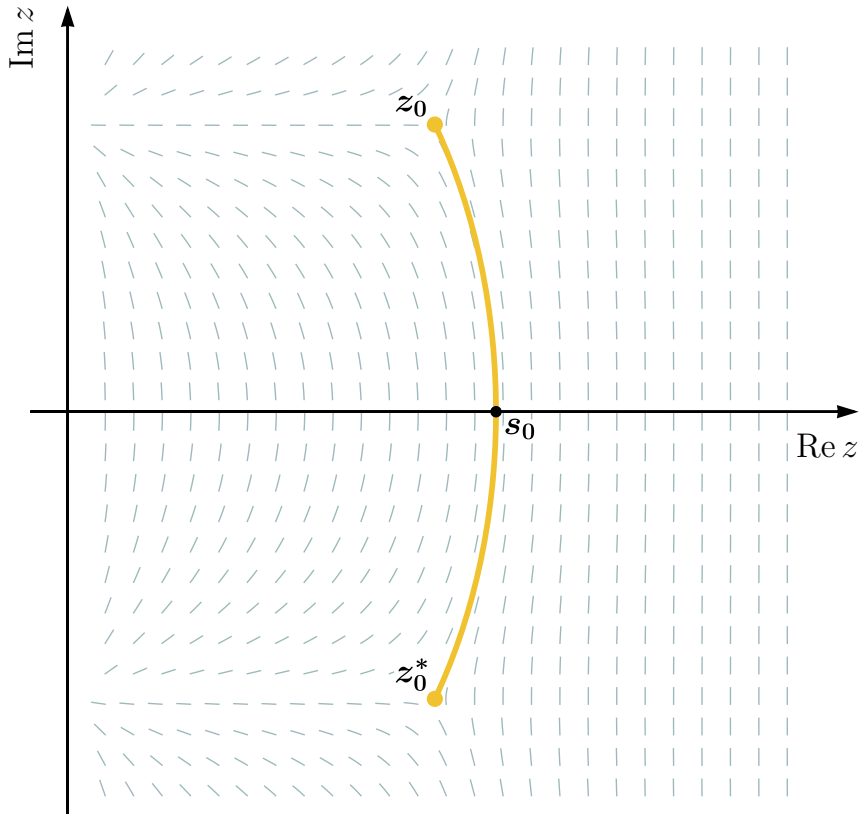

Figure 10: A depiction of the Stokes line sourced by a conjugate pair of simple turning points $\left(z_0,\, z_0^*\right)$ of a frequency function $\Omega_k(z)$. Here the Stokes line crosses the real axis at the point s_0, which corresponds to the time at which particle production occurs for the mode of wavenumber k. The guiding lines show the directions for which the condition $\mathrm{Re}\left[\Omega_k \mathrm{d}z\right] = 0$ is locally satisfied.

motion for a given field mode extended to a complex time variable z:

$$f_k''(z) + \Omega_k^2(z) f_k(z) = 0\,, \tag{3.12}$$

in which the primes stand for differentiation with respect to z, the proper time is given by $t \equiv \mathrm{Re}\, z$, and $\Omega_k(z)$ represents the analytic continuation of the time-dependent frequency of Eq. (1.29). The Stokes lines associated with Eq. (3.12) are those lines which emanate from the zeros (also known as turning points) and poles of $\Omega_k(z)$ and along which $\mathrm{Re}\big[\Omega_k \mathrm{d}z\big] = 0$. An illustration of such a line is shown in Fig. 10. The asymptotic solutions susceptible to the Stokes phenomenon are given by

$$f_k(z) = \alpha_k(z) h_k(z) + \beta_k(z) h_k^*(z)\,, \tag{3.13}$$

where $h_k(z)$ and $h_k^*(z)$ are the complex extensions of the adiabatic mode functions defined in the previous section. As this solution evolves across a Stokes line, the values of the Bogolyubov coefficients $\alpha_k(z)$ and $\beta_k(z)$ change abruptly. By Eqs. (3.10) and (3.11), this implies a sudden change in the adiabatic bilinears and, in particular, the production of adiabatic particles. Remarkably, a result from asymptotic analysis guarantees the existence of a smooth universal form for this rapid transition between different asymptotic regimes. Below we outline the derivation of this important result and summarize the quantities which determine the functional form of such smooth Stokes jumps.

We start by defining Dingle's singulant variable [100] anchored at z_0:

$$F_k^{(0)}(z) = 2i \int_{z_0}^{z} \Omega_k(w)\, \mathrm{d}w\,, \tag{3.14}$$

where z_0 is a solution of $\Omega_k(z) = 0$ which sources the Stokes line of interest, is closest to the real axis, and is located in the upper half-plane. The singulant is a convenient variable for tracking the change incurred by the Bogolyubov coefficients $\alpha_k(z)$ and $\beta_k(z)$ across a Stokes line. Indeed, it was shown by Berry [101–104] that these coefficients satisfy the following differential equations in the vicinity of a Stokes line:

$$\frac{d\beta_k}{dF_k^{(0)}} = C_{\beta,\,k}^{(0)}\, \alpha_k\,, \tag{3.15a}$$

$$\frac{d\alpha_k}{dF_k^{(0)}} = C_{\alpha,\,k}^{(0)}\,\beta_k\,, \tag{3.15b}$$

where $C_{\beta,\,k}^{(0)}$ and $C_{\alpha,\,k}^{(0)}$ are coupling functions which depend on the order at which the series representation of $W_k(z)$ is truncated. A remarkable discovery by Dingle [100] states that the large-order terms in the asymptotic series of Eq. (3.2) have a closed form given by

$$\psi_{k,\,2n}(z) \sim -\frac{(2n-1)!}{\pi F_k^{(0)\,2n}} \quad \text{for} \quad n \gg 1\,. \tag{3.16}$$

It is clear from this result that the smallest term in such a series corresponds to $n \approx \left|F_k^{(0)}\right|$. Terminating the series at this order leads to optimal closed form expressions for $C_{\beta,\,k}^{(0)}$ and $C_{\alpha,\,k}^{(0)}$, which can be substituted in Eqs. (3.15) to yield the following universal behaviors for $\beta_k(t)$ and $\alpha_k(t)$ along the real axis and across the Stokes line under consideration:

$$\beta_k(t) \approx \frac{i}{2}\,\mathrm{Erfc}\Big(-\vartheta_k^{(0)}(t)\Big)\delta_k^{(0)}\,, \tag{3.17a}$$

$$\alpha_k(t) \approx \sqrt{1+\left|\beta_k(t)\right|^2}\,, \tag{3.17b}$$

where $\vartheta_k^{(0)}(t)$ is a natural time evolution parameter which determines the sharpness of the Stokes jump, and $\delta_k^{(0)}$ corresponds to the jump's amplitude. Both of these parameters are expressible in terms of the singulant variable evaluated over the real axis:

$$\vartheta_k^{(0)}(t) = \frac{\mathrm{Im}\Big[F_k^{(0)}(t)\Big]}{\sqrt{2\,\mathrm{Re}\Big[F_k^{(0)}(t)\Big]}}\,, \tag{3.18a}$$

$$\delta_k^{(0)} = \exp\Big(-F_k^{(0)}(s_0)\Big)\,. \tag{3.18b}$$

Here $F_k^{(0)}(s_0)$ is simply the singulant computed at the point $z = s_0$, where the Stokes line sourced by z_0 intersects the real axis, i.e.,

$$F_k^{(0)}(s_0) = 2i\int_{z_0}^{s_0}\Omega_k(w)\,\mathrm{d}w = i\int_{z_0}^{z_0^*}\Omega_k(w)\,\mathrm{d}w\,, \tag{3.19}$$

where the last equality follows from the reality of $\Omega_k(z)$ over the real axis. Putting together Eqs. (3.10), (3.11), and (3.17) yields a universal functional form which describes the time

evolution of the adiabatic bilinears associated with the field mode of wavenumber k:

$$\mathcal{N}_k \approx N_k + \frac{\sigma_k}{4}\left|\mathrm{Erfc}\Big(-\vartheta_k^{(0)}\Big)\delta_k^{(0)}\right|^2, \tag{3.20a}$$

$$\mathcal{M}_k \approx -i\,\frac{\sigma_k}{2}\left[\mathrm{Erfc}\Big(-\vartheta_k^{(0)}\Big)\delta_k^{(0)}\right]\left[1+\mathcal{N}_k\right]^{1/2}. \tag{3.20b}$$

These results can be further generalized to account for multiple Stokes line crossings, as well as the interference effects between them [98]. Define the accumulated phase between the first and the p-th pair of zeros of $\Omega_k(z)$ as

$$\theta_k^{(p)} = \int_{s_0}^{s_p} \Omega_k(w)\,\mathrm{d}w \tag{3.21}$$

where s_p corresponds to the point where the Stokes line associated with the p-th conjugate pair of zeros crosses the real axis. The functions which describe both adiabatic bilinears are then given by

$$\mathcal{N}_k \approx N_k + \frac{\sigma_k}{4}\left|\sum_p \mathrm{Erfc}\Big(-\vartheta_k^{(p)}\Big)\delta_k^{(p)}\exp\Big(2i\theta_k^{(p)}\Big)\right|^2, \tag{3.22a}$$

$$\mathcal{M}_k \approx -i\,\frac{\sigma_k}{2}\left[\sum_p \mathrm{Erfc}\Big(-\vartheta_k^{(p)}\Big)\delta_k^{(p)}\exp\Big(-2i\theta_k^{(p)}\Big)\right]\left[1+\mathcal{N}_k\right]^{1/2} \tag{3.22b}$$

with $\delta_k^{(p)}$ and $\vartheta_k^{(p)}(t)$ being the amplitude and time evolution parameter associated with the p-th Stokes line.

Therefore, by monitoring the turning points and Stokes lines which accompany each mode's frequency function on the complex plane, we can track the evolution of the adiabatic bilinears related to any physically acceptable field state. In the next section we examine how this evolution affects the Universe's scale factor through the semi-classical Einstein equations.

3.4 THE SEMI-CLASSICAL EINSTEIN EQUATIONS

If cosmological quantum particle production occurs at a sufficiently high rate, it can in principle back-react on the cosmic evolution through the semi-classical Einstein equations

$$R_{ab} - \frac{1}{2} R\, g_{ab} + \Lambda\, g_{ab} = m_P^{-2} \langle \hat{T}_{ab} \rangle \tag{3.23}$$

where Λ represents the cosmological constant, $m_P = (8\pi G)^{-1/2}$ stands for the reduced Planck mass, and $\langle \hat{T}_{ab} \rangle$ corresponds to the expectation value of the energy-momentum tensor operator, including contributions both from the scalar field we are considering plus any other stress-energy sources. The canonical expression for $\hat{T}_{ab}$ due to the scalar field is constructed by varying the action in Eq. (1.23) with respect to the metric g_{ab}, and subsequently substituting the field operator $\hat{\Phi}$ from Eq. (1.25) into the resulting expression:

$$\hat{T}_{ab} = \big(\nabla_a \hat{\Phi}\big)\big(\nabla_b \hat{\Phi}\big) - \frac{1}{2} g_{ab} \big(\nabla^c \hat{\Phi}\big)\big(\nabla_c \hat{\Phi}\big) + \xi \left[g_{ab}\, \Box - \nabla_a \nabla_b + R_{ab} - \frac{1}{2} R\, g_{ab} - \frac{m^2}{2} g_{ab} \right] \hat{\Phi}^2 \,. \tag{3.24}$$

For a statistically homogeneous and isotropic field state, $\langle \hat{T}_{ab} \rangle$ is equivalent to the energy-momentum tensor of a perfect fluid for which the field energy density and pressure are given, respectively, by $\rho(t) = \langle \hat{T}_{00} \rangle$ and $P(t) = \frac{1}{3} g^{ij} \langle \hat{T}_{ij} \rangle$. As a consequence, such a state naturally sources an FLRW metric, reducing Eq. (3.23) to the usual Friedmann equations:

$$H^2(t) = \frac{1}{3} m_P^{-2} \rho(t) + \frac{\Lambda}{3} - \frac{K}{a^2(t)} \tag{3.25a}$$

$$\dot{H}(t) + H^2(t) = -\frac{1}{6} m_P^{-2} \Big[\rho(t) + 3P(t) \Big] + \frac{\Lambda}{3} \,. \tag{3.25b}$$

Furthermore, it can be shown that $\langle \hat{T}_{ab} \rangle$ is covariantly conserved, resulting in the cosmological continuity equation

$$\dot{\rho}(t) + 3H(t) \Big[\rho(t) + P(t) \Big] = 0 \,. \tag{3.26}$$

However, at this stage these equations are merely formal, because both the pressure and energy density of a quantized field are in general divergent and need to be regularized. In a FLRW spacetime, these divergencies can be partially isolated by expressing $\rho(t)$ and $P(t)$ in terms of the adiabatic bilinears $\mathcal{N}_k(t)$ and $\mathcal{M}_k(t)$ [94]. Substituting Eqs. (1.25), (3.5), and

(3.6) into the expectation value of Eq. (3.24) and collecting terms with the same adiabatic factor gives

$$\rho(t) = \langle \hat{T}_{00} \rangle = \frac{1}{4\pi a^3(t)} \int \mathrm{d}\mu(k) \left\{ \rho_k^{\mathcal{N}}(t) \left[\mathcal{N}_k(t) + \frac{1}{2} \right] + \rho_k^{\mathcal{R}}(t)\, \mathcal{R}_k(t) + \rho_k^{\mathcal{I}}(t)\, \mathcal{I}_k(t) \right\} \tag{3.27a}$$

$$P(t) = \frac{1}{3} g^{ij} \langle \hat{T}_{ij} \rangle = \frac{1}{4\pi a^3(t)} \int \mathrm{d}\mu(k) \left\{ P_k^{\mathcal{N}}(t) \left[\mathcal{N}_k(t) + \frac{1}{2} \right] + P_k^{\mathcal{R}}(t)\, \mathcal{R}_k(t) + P_k^{\mathcal{I}}(t)\, \mathcal{I}_k(t) \right\}. \tag{3.27b}$$

The terms proportional to $\mathcal{N}_k(t)$ capture the contribution to the energy density and pressure due to the evolving distribution of adiabatic particles populating the field modes, while the quantum interference terms contain $\mathcal{R}_k(t) = \mathrm{Re}\big[\mathcal{M}_k(t)\big]$ and $\mathcal{I}_k(t) = \mathrm{Im}\big[\mathcal{M}_k(t)\big]$ *. The prefactors in each of these terms are defined as

$$\rho_k^{\mathcal{N}}(t) \equiv \frac{1}{W_k(t)} \left\{ W_k^2(t) + \omega_k^2(t) + \frac{1}{4}\Big[V_k(t) - H(t)\Big]^2 + \right. \tag{3.28a}$$
$$\left. + \big(6\xi - 1\big) \left[H(t) V_k(t) - 2H^2(t) + \frac{K}{a^2(t)} \right] \right\},$$

$$\rho_k^{\mathcal{R}}(t) \equiv \frac{1}{W_k(t)} \left\{ - W_k^2(t) + \omega_k^2(t) + \frac{1}{4}\Big[V_k(t) - H(t)\Big]^2 + \right. \tag{3.28b}$$
$$\left. + \big(6\xi - 1\big) \left[H(t) V_k(t) - 2H^2(t) + \frac{K}{a^2(t)} \right] \right\},$$

$$\rho_k^{\mathcal{I}}(t) \equiv V_k(t) - H(t) + 2H(t)\big(6\xi - 1\big), \tag{3.28c}$$

$$P_k^{\mathcal{N}}(t) \equiv \frac{1}{3W_k(t)} \left\{ W_k^2(t) + \omega_k^2(t) - 2m^2 + \frac{1}{4}\Big[V_k(t) - H(t)\Big]^2 + \frac{1}{3}\big(6\xi - 1\big)^2 R(t) + \right.$$
$$+ \big(6\xi - 1\big) \left[- 2W_k^2(t) - \frac{1}{2} V_k^2(t) + 4H(t) V_k(t) + 2\omega_k^2(t) + \right. \tag{3.28d}$$
$$\left. \left. + 2\dot{H}(t) + \frac{K}{a^2(t)} - \frac{5}{2} H^2(t) \right] \right\},$$

*Here the definitions for $\mathcal{R}_k(t)$ and $\mathcal{I}_k(t)$ might seem to differ from those found in the literature by a phase factor, but this factor is implicit in our definitions for $\alpha_k(t)$ and $\beta_k(t)$ obtained from asymptotic analysis

$$P_k^{\mathcal{R}}(t) \equiv \frac{1}{3W_k(t)}\Bigg\{ -W_k^2(t) + \omega_k^2(t) - 2m^2 + \frac{1}{4}\Big[V_k(t) - H(t)\Big]^2 + \frac{1}{3}\big(6\xi - 1\big)^2 R(t) +$$

$$+ \big(6\xi - 1\big)\Bigg[2W_k^2(t) - \frac{1}{2}V_k^2(t) + 4H(t)V_k(t) + 2\omega_k^2(t) + 2\dot{H}(t) + \tag{3.28e}$$

$$+ \frac{K}{a^2(t)} - \frac{5}{2}H^2(t)\Bigg]\Bigg\},$$

$$P_k^{\mathcal{I}}(t) \equiv \frac{1}{3}\Big[V_k(t) - H(t)\Big] + \frac{2}{3}\big(6\xi - 1\big)\Big[4H(t) - V_k(t)\Big]. \tag{3.28f}$$

For adiabatic field states, the contributions to the energy density and pressure due to the real bilinears $\mathcal{N}_k(t)$, $\mathcal{R}_k(t)$, and $\mathcal{I}_k(t)$ are always finite. This implies that the divergencies in Eqs. (3.27a) and (3.27b) are isolated in the vacuum-like terms characterized by the $\frac{1}{2}$ factors, henceforth identified as

$$\rho_{\rm vac}(t) \equiv \frac{1}{8\pi a^3(t)}\int \mathrm{d}\mu(k)\, \rho_k^{\mathcal{N}}(t) \tag{3.29a}$$

$$P_{\rm vac}(t) \equiv \frac{1}{8\pi a^3(t)}\int \mathrm{d}\mu(k)\, P_k^{\mathcal{N}}(t)\,. \tag{3.29b}$$

Regularization consists precisely in controlling the divergent behavior of $\rho_{\rm vac}(t)$ and $P_{\rm vac}(t)$ so as to obtain finite expressions for $\rho(t)$ and $P(t)$ which still satisfy the cosmological continuity equation. Adiabatic regularization achieves this result by subtracting the fourth-order phase-integral expansions of $\rho_k^{\mathcal{N}}(t)$ and $P_k^{\mathcal{N}}(t)$ from the integrands of Eqs. (3.29a) and (3.29b), respectively [79, 84]. From a technical perspective, however, this procedure introduces significant challenges to the numerical implementation of the semi-classical Friedmann equations. Chief among these is the appearance of higher-order time derivatives of $H(t)$ in the integrands of Eqs. (3.27), turning the semi-classical Friedmann equations into a system of integro-differential equations which is not amenable to standard numerical treatments. We circumvent this difficulty by employing an alternative regularization scheme which, albeit cruder, yields a good approximation to $\rho(t)$ and $P(t)$ in regimes dominated by particle production.

Central to the regularization approach adopted here is the realization that $\rho_{\rm vac}(t)$ and $P_{\rm vac}(t)$ independently satisfy the cosmological continuity equation as long as the function

$V_k(t)$ has the form established in Eq. (3.7) (see the Appendix). It follows that the vacuum contributions to $\rho(t)$ and $P(t)$ can be discarded in their entirety while still ensuring that Eq. (3.26) remains valid. Despite its simplicity, this procedure yields a good approximation to the field energy density and pressure provided the adiabatically regularized integrands of Eqs. (3.27) are dominated by the real adiabatic bilinears $\mathcal{N}_k(t)$, $\mathcal{R}_k(t)$, and $\mathcal{I}_k(t)$. Therefore, in what follows we take the regularized expressions for the energy density and pressure to be

$$\rho(t) \approx \frac{1}{4\pi a^3(t)} \int \mathrm{d}\mu(k) \left\{ \rho_k^{\mathcal{N}}(t)\, \mathcal{N}_k(t) + \rho_k^{\mathcal{R}}(t)\, \mathcal{R}_k(t) + \rho_k^{\mathcal{I}}(t)\, \mathcal{I}_k(t) \right\} \tag{3.30a}$$

$$P(t) \approx \frac{1}{4\pi a^3(t)} \int \mathrm{d}\mu(k) \left\{ P_k^{\mathcal{N}}(t)\, \mathcal{N}_k(t) + P_k^{\mathcal{R}}(t)\, \mathcal{R}_k(t) + P_k^{\mathcal{I}}(t)\, \mathcal{I}_k(t) \right\}, \tag{3.30b}$$

where the factors $\rho_k^{\mathcal{N}}(t)$, $\rho_k^{\mathcal{R}}(t)$, and $\rho_k^{\mathcal{I}}(t)$, $P_k^{\mathcal{N}}(t)$, $P_k^{\mathcal{R}}(t)$, and $P_k^{\mathcal{I}}(t)$ are computed by truncating the asymptotic series Eq. (3.2) for $W_k(t)$ at its optimal order.

Finally, the regularization of $\langle \hat{T}_{ab} \rangle$ also induces the renormalization of the gravitational coupling constants G and Λ. Moreover, self-consistency demands the introduction of a covariantly conserved tensor composed of fourth-order derivatives of the metric into the semi-classical Einstein equations [80, 81]. This tensor is accompanied by a new unknown coupling constant whose renormalization assimilates the ultra-violet divergence in the field energy-momentum tensor. For simplicity, in this work we assume this new coupling constant to be renormalized to zero, thus preserving the form of Eq. (3.23). Non-zero values for this coupling constant will be considered elsewhere.

Taken together, Eqs. (3.22), (3.25), and (3.30) describe the coupled field evolution and cosmic evolution in regimes dominated by particle production. In the next section we present an algorithm which numerically solves this system of equations.

3.5 NUMERICAL IMPLEMENTATION

The semi-classical Friedmann equations can be formulated as a discretized initial value problem. We take the domain of numerical integration to be a band of the complex plane which is bisected by the real t axis. As illustrated in Figure 11, this band is discretized by a uniformly spaced grid where the real-valued entries t_j label the physical time. Initial conditions are set by an appropriately chosen functional form for the scale factor $a(t)$ which not only admits an adiabatic field state at the initial time t_0, but which is also consistent with our choice for the initial distribution of adiabatic particles $\mathcal{N}_k(t_0) = N_k$ populating the field modes. In addition, we require that

$$N_k < \mathcal{O}(k^{-3}) \quad \text{as} \quad k \longrightarrow \infty \tag{3.31}$$

in order to ensure that both the energy density and pressure associated with the initial particle distribution are finite.

We use a standard finite-difference scheme to step $a(t)$, $H(t)$, and $\dot{H}(t)$ along the real axis, and employ B-splines to scan the Stokes geometry on the complex plane. The latter is accomplished by generating a numerical sample of $\Omega_k(t)$ through Eq. (1.29), and subsequently performing high-order B-spline interpolations to construct a truncated Taylor polynomial for this function over the real line up to the value of t in the current time step. Due to the analyticity of $\Omega_k(t)$, this series representation is also valid on the complex plane, and thus encodes the analytical continuation of the frequency function. Explicitly, given a grid point z_{ij} on the discretized plane, we compute $\Omega_k(z_{ij})$ through the expression

$$\Omega_k(z_{ij}) \approx \sum_{n=0}^{T} \frac{1}{n!} \big(z_{ij} - t_j\big)^n \, \Omega_k^{(n)}(t_j) \,, \tag{3.32}$$

where $t_j = \operatorname{Re} z_{ij}$, as depicted in Figure 11. The numerical derivatives $\Omega_k^{(n)}$ are extracted from B-spline interpolations over the real axis, and T corresponds to a truncation order which depends on the density of grid points lying over the real axis. In addition, we feed Eq. (3.32) to a Padé approximant [107] routine to accelerate its convergence and improve its accuracy. Once this approximate representation of the frequency function has been computed over the discretized plane, it can be interpolated and used in the monitoring of turning points and

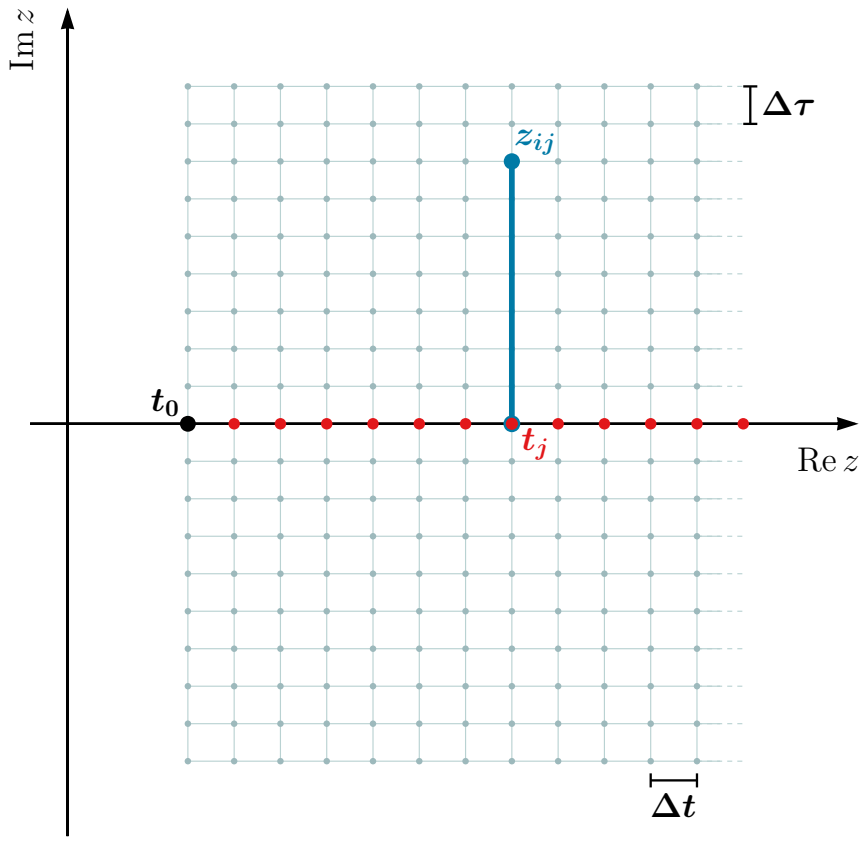

Figure 11: A grid of uniformly spaced points covering a band of the complex plane. The grid points lying over the real axis mark the discretization of physical time. Numerically constructing the Taylor polynomial associated with the frequency function around the point t_j allows for the optimal evaluation of $\Omega_k(z_{ij})$ at grid points z_{ij} for which $\mathrm{Re}\, z_{ij} = t_j$.

Stokes lines.

While the turning points of $\Omega_k(z)$ can be located with the aid of root-finding algorithms designed for multi-valued functions, the problem of determining the Stokes lines sourced by these points requires the numerical integration of an ordinary differential equation. This is evident from the Stokes lines definition $\mathrm{Re}\big[\Omega_k \mathrm{d}z\big] = 0$, which implies that, locally, its line element must satisfy $\mathrm{d}z \propto i/\Omega_k(z)$. Defining $t = \mathrm{Re}\, z$ and $\tau = \mathrm{Im}\, z$, this condition can be rewritten as

$$\mathrm{d}z = \mathrm{d}t + i\,\mathrm{d}\tau \propto \frac{i}{\Omega_k(z)}\,. \tag{3.33}$$

Taking the ratio between the matched real and imaginary parts of this proportionality relation leads to the differential equation

$$\frac{dt}{d\tau} = \frac{\mathrm{Im}\,\Omega_k(z)}{\mathrm{Re}\,\Omega_k(z)} \tag{3.34}$$

for the Stokes line, which can be numerically integrated from the turning point of interest to yield $t(\tau)$.

Here is a summary of the minimal set of tasks performed by our algorithm while evolving the physical quantities of interest by one time step:

1. Take samples of $a(t)$, $H(t)$, and $\dot{H}(t)$ describing the metric along an interval of the real axis. Over this same interval, sample and interpolate the field energy density $\rho(t)$ and pressure $P(t)$.
2. Numerically integrate the semi-classical Friedmann equations so as to enlarge the input metric samples $a(t)$, $H(t)$, and $\dot{H}(t)$ by a time step Δt.
3. For each field mode, generate a sample of the frequency function $\Omega_k(t)$ over the real axis, and numerically extend this function onto the complex plane to obtain $\Omega_k(z)$.
4. Search for complex turning points of each frequency function $\Omega_k(z)$, and numerically trace their corresponding Stokes lines.
5. If a Stokes line associated with a mode of wavenumber k is found to intersect the real axis, update the real bilinears $\mathcal{N}_k(t)$, $\mathcal{R}_k(t)$ and $\mathcal{I}_k(t)$ accordingly.
6. For each field mode, compute $W_k(t)$ and $V_k(t)$ up to the optimal truncation order set by the last Stokes line crossing.

7. Gather the results from all previous steps to evolve the input samples for the field energy density $\rho(t)$ and pressure $P(t)$ by a time step Δt.

In general, the Stokes lines associated with field modes of comparable wavenumber will cross the real axis within close proximity of one another, giving rise to overlapping particle production events. In order to correctly capture the influence that such events might have on each other, we apply the stepping algorithm outlined above in an iterative fashion. In other words, once the quantities of interest have been forward-stepped up to t_j, the following iteration backtracks to t_0 and then proceeds to step the problem up to $t_{j+1} = t_j + \Delta t$ using as sources for the semi-classical Friedmann equations the field energy density and pressure obtained in the previous iteration.

In summary, our numerical implementation allows for the scale factor and the Stokes geometry to reconfigure themselves with each iteration and thereby construct a self-consistent solution to the back-reaction problem.

3.6 NUMERICAL RESULTS

To assess the accuracy of our numerical approach, we first neglect back-reaction effects and compare numerical results to known analytic solution for a quantized scalar field evolving in a closed de Sitter spacetime [108]. This case is characterized by a positive cosmological constant Λ and a curvature parameter of $K = 1$, which together lead to a bouncing scale factor evolution

$$a(t) = \bar{H}^{-1} \cosh\left(\bar{H}t\right) \quad \text{with} \quad \bar{H} = \sqrt{\Lambda/3}\,. \tag{3.35}$$

Here $\bar{H}$ is the asymptotic value of the Hubble parameter in the infinite future,

$$\lim_{t\to\pm\infty} H(t) = \pm\bar{H}\,. \tag{3.36}$$

This model Universe contracts for $t < 0$, reaches its minimum size at $t = 0$, and subsequently expands for the $t > 0$.

Substituting Eq. (3.35) into Eq. (1.29) yields

$$\Omega_k^2(t) = \bar{H}^2\left[\left(k^2 - \frac{1}{4}\right)\operatorname{sech}^2\left(\bar{H}t\right) + \frac{m^2}{\bar{H}^2} + 12\,\xi - \frac{9}{4}\right] \tag{3.37}$$

for the mode frequency function. Analytically extending this function to the complex plane, locating its turning points, and tracing its Stokes lines are straightforward. We verify our numerical calculations against these analytic results. For definiteness, we choose a scalar field mass $m = 0.1\,m_P$ which is conformally coupled to the scalar curvature, $\xi = \frac{1}{6}$. We set the cosmological constant to $\Lambda = 3\,m^2$, so that $\bar{H} = 1\,m$. All dimensional quantities are thus expressed in terms of the field mass.

A comparison between the analytic extension of Eq. (3.37) and the numerical analytic continuation produced by our algorithm is displayed in Figure 12 for the field mode of wavenumber $k = 5\,m$. The left panel shows the absolute value of the numerically obtained frequency function, while the right panel exhibits how this result deviates from the analytic expression for $\Omega_k(z)$. In addition to correctly reproducing the function's conjugate pair of zeroes $\left(z_0,\, z_0^*\right)$ located in this region, the numerical analytic continuation differs from the analytic value by at most 2% in the vicinity of these points. As a result, the Stokes lines which occupy this area of the complex plane can be traced with high fidelity. This is demonstrated in the left panel of Figure 13, where the Stokes lines sourced by the pairs of turning points $\left(z_0,\, z_0^*\right)$ and $\left(z_1,\, z_1^*\right)$ are superimposed over the numerically obtained frequency function. The effects of each Stokes line on the adiabatic bilinear $\mathcal{N}_k(t)$ are displayed in the right panel of Figure 13, wherein this quantity is tracked as a function of time. Each burst of particle production is prompted by a Stokes line crossing, the first of which occurs as the Universe contracts and the field mode under consideration becomes sub-horizon; while the second burst happens after the bounce, when the mode reverts back to being super-horizon due to the Universe's expansion [94]. Despite the symmetry between these events, constructive interference expressed by Eq. (3.22) causes more particles to be produced in the second burst. The expected values for the particle number plateaus are indicated by the square markers on the vertical axis, both of which agree well with the numerical curve.

By tracing the Stokes geometry of every field mode, we can also track the evolution of the

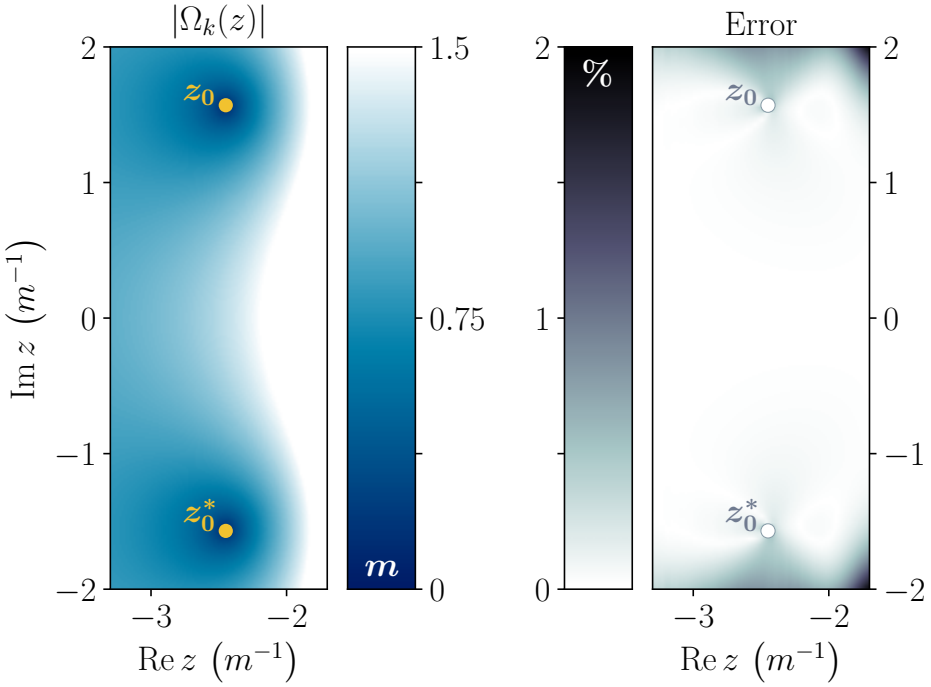

Figure 12: A comparison between the numerical analytic continuation of $\Omega_k(z)$ produced by our algorithm and the expected analytic expression for this function in a closed de Sitter spacetime. The field parameters are $m = 0.1\,M$, $\xi = \frac{1}{6}$, and $k = 5\,m$, while the spacetime is characterized by $\Lambda = 3\,m^2$ and $K = 1$. The left panel shows the absolute value of the numerically produced frequency function in the vicinity of the pair of conjugate turning points $\left(z_0,\, z_0^*\right)$, while the right panel exhibits the relative difference between the analytic and numerical results.

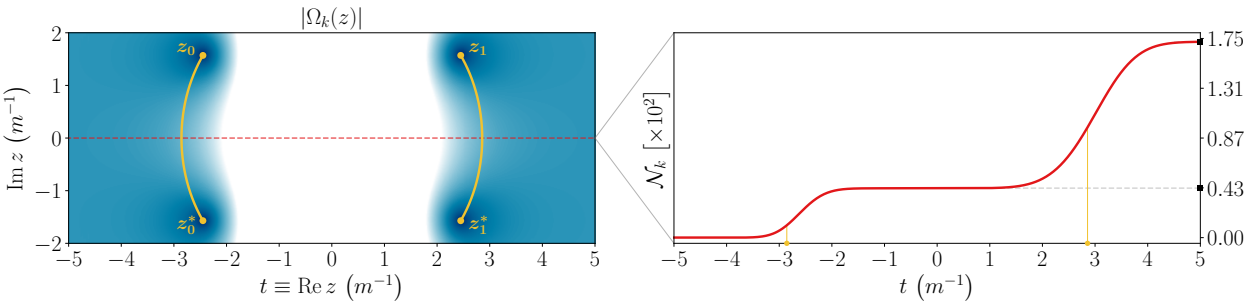

Figure 13: The numerically traced Stokes geometry associated with the frequency function $\Omega_k(z)$, and the adiabatic particle number evolution $\mathcal{N}_k(t)$ extracted from it. The field parameters are set to $m = 0.1\, m_P$, $\xi = \frac{1}{6}$, $k = 5\, m$, and $N_k = 0$, while the spacetime is characterized by $\Lambda = 3\, m^2$ and $K = 1$. The left panel shows the Stokes lines sourced by the pairs of turning points $\left(z_0,\, z_0^*\right)$ and $\left(z_1,\, z_1^*\right)$ superimposed over the absolute value of the numerically obtained frequency function. The real axis corresponds to the central dashed line. The effects of each Stokes line on the adiabatic particle number $\mathcal{N}_k(t)$ are illustrated on the right panel, wherein this quantity is tracked as a function of time. Each burst of particle production is prompted by a Stokes line crossing, indicated here by the circular markers on the horizontal axis. The expected values for the particle number plateaus featuring in this image are indicated by the square markers on the vertical axis, both of which show very good agreement with the numerically produced curve for $\mathcal{N}_k(t)$. Constructive interference causes more particles to be produced in the second burst.

field energy density as the spacetime evolves. Even though back-reaction effects are being neglected, this quantity shows whether the effects of particle production will eventually become comparable to the contributions from Λ and K which source the background de Sitter spacetime. To that end, we track every term appearing on the right-hand side of the semi-classical Friedmann Eq. (3.25a), identifying each contribution according to the notation

$$H^2_{\mathcal{N},\mathcal{R},\mathcal{I}} \equiv \frac{\rho}{3m_P^2}\,, \quad H^2_{\Lambda} \equiv \frac{\Lambda}{3}\,, \quad \text{and} \quad H^2_{K} \equiv -\frac{K}{a^2}\,. \tag{3.38}$$

Additionally, we define $H^2_{\mathcal{R},\mathcal{I}}$ as the contribution to the right-hand side of Eq. (3.25a) which stems solely from terms proportional to the real bilinears $\mathcal{R}_k$ and $\mathcal{I}_k$. The left panel of Figure 14 displays the evolution of the above-defined quantities for a bounce that starts at $t_0 = -5\,m^{-1}$ with an initial particle distribution given by $\mathcal{N}_k(t_0) = 0$. Being the only true sources in this case, H^2_{Λ} and H^2_{K} behave in the standard way, acting in concert to produce the de Sitter bounce. Because back-reaction effects are neglected, the Hubble parameter H shown on the right panel of Figure 14 is entirely characterized by these two quantities, i.e., $H^2 = H^2_{\Lambda} + H^2_{K}$. On the other hand, the field-related quantities $H^2_{\mathcal{N},\mathcal{R},\mathcal{I}}$ and $H^2_{\mathcal{R},\mathcal{I}}$ display an interesting behavior which mirrors the result found in Ref. [95]. While $H^2_{\mathcal{R},\mathcal{I}}$ remains negligible throughout, $H^2_{\mathcal{N},\mathcal{R},\mathcal{I}}$ grows exponentially as the Universe progresses toward the bounce. In other words, the field energy density eventually becomes dominated by $\mathcal{N}_k$ – the field particle content. Physically, the soaring field energy density is due to the blueshift experienced by particles produced in the contracting phase. As a result, the Universe is filled with relativistic particles which effectively behave as radiation, making the field energy density grow as $\rho \propto a^{-4}$. This trend is then reversed in the ensuing expanding phase, during which the field energy density drops rapidly as particles are continuously redshifted.

The preceding calculations demonstrate that back-reaction effects due to particle production can become dynamically significant in an initially closed de Sitter spacetime. A full account of these effects is shown in Figure 15, using the algorithm for computing back-reaction effects described in the previous Section. In this case, the metric evolution initially matches that of a closed de Sitter spacetime at $t_0 = -5\,m^{-1}$, while the initial particle distribution is given by $\mathcal{N}_k(t_0) = 0$. These initial conditions self-consistently satisfy the semi-classical Friedmann equations at the initial time t_0 within our approximations. As in the case

without back reaction, the quantity $H^2_{\mathcal{R},\mathcal{I}}$ remains sub-dominant throughout the evolution, while $H^2_{\mathcal{N},\mathcal{R},\mathcal{I}}$ grows exponentially as newly-created particles are continuously blueshifted. Since they quickly become relativistic, these particles behave as an additional radiation-like component, destabilizing the initial de Sitter phase. This is illustrated in the right panels of Figure 15,where the scale factor and Hubble parameter can be seen transitioning from a de Sitter bounce to a radiation-dominated behavior. The contributions from the regularized vacuum terms discarded in our approximations remain negligible at all times. We stop the numerical integration at $t = -1.3\, m^{-1}$, since beyond this time the Hubble parameter becomes of order $H \simeq m_P^{-1}$, invalidating the semi-classical picture of gravity on which our calculations rely.

The de Sitter bounce is not always disrupted by particle production. For sufficiently low values of the field mass, the bounce is merely delayed. Figure 16 illustrates a near-limiting case with $m = 0.0145\, m_P$ for which an initial de Sitter evolution is still driven toward a radiation dominated phase. The contributions due to particle production $H^2_{\mathcal{N},\mathcal{R},\mathcal{I}}$ only come to dominate over the combined H^2_Λ and H^2_K near the bounce at $t = 0\, m^{-1}$. For field masses $m \lesssim 0.0142\, m_P$, the negative curvature contributions H^2_K neutralize the growth of $H^2_{\mathcal{N},\mathcal{R},\mathcal{I}}$ for long enough to preserve the bounce. The resulting bounce is pushed to a slightly later time and occurs at a smaller value of the scale factor.

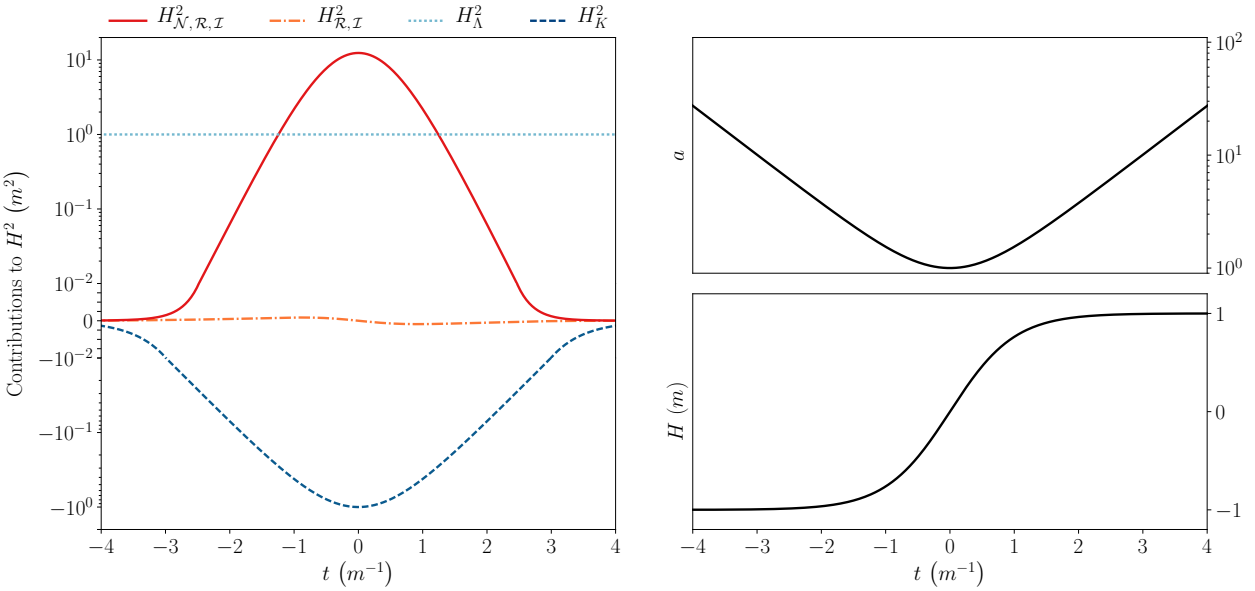

Figure 14: The evolution of every term appearing on the right-hand side of the semi-classical Friedmann Eq. (3.25a) in a closed de Sitter spacetime evolution, as well as the quantities describing the metric for this spacetime in the absence of back-reaction. The field parameters are set to $m = 0.1\, m_P$ and $\xi = \frac{1}{6}$, while the spacetime is characterized by $\Lambda = 3\, m^2$ and $K = 1$. The bounce starts at $t_0 = -5\, m^{-1}$ with an initial particle distribution given by $\mathcal{N}_k(t_0) = 0$. The left panel follows the evolution of $H^2_{\mathcal{N},\mathcal{R},\mathcal{I}}$ (solid line), $H^2_{\mathcal{R},\mathcal{I}}$ (dot-dashed line), H^2_Λ (dotted line), and H^2_K (dashed line). While $H^2_{\mathcal{R},\mathcal{I}}$ remains negligible throughout, $H^2_{\mathcal{N},\mathcal{R},\mathcal{I}}$ grows exponentially and eventually comes to dominate over all other contributions. The right panels illustrate the scale factor $a(t)$ and Hubble parameter $H(t)$ which describe the de Sitter bounce. Because back-reaction effects are being neglected, the Hubble parameter is just $H^2 = H^2_\Lambda + H^2_K$.

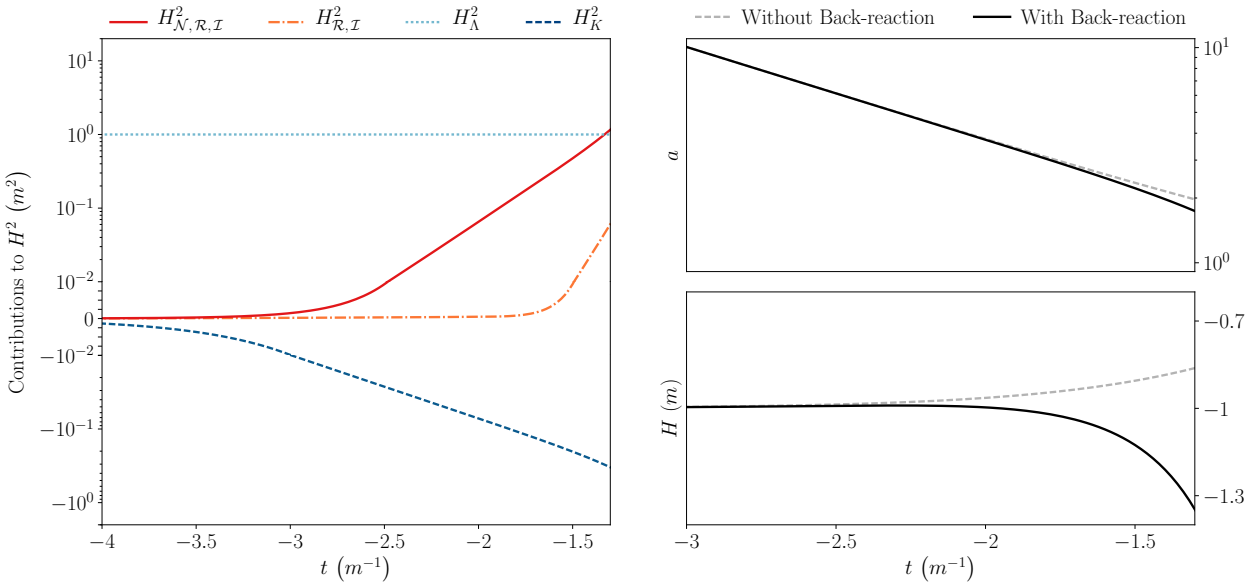

Figure 15: The evolution of every term appearing on the right-hand side of the semi-classical Friedmann Eq. (3.25a) and the quantities describing the metric evolution in a full back-reacting calculation. The field parameters are $m = 0.1\, m_P$ and $\xi = \frac{1}{6}$, while the cosmological constant and curvature parameter are $\Lambda = 3\, m^2$ and $K = 1$. The closed de Sitter initial conditions are set at $t_0 = -5\, m^{-1}$, along with an initial particle distribution given by $\mathcal{N}_k(t_0) = 0$. The left panel follows the evolution of $H^2_{\mathcal{N},\mathcal{R},\mathcal{I}}$ (solid line), $H^2_{\mathcal{R},\mathcal{I}}$ (dot-dashed line), H^2_Λ (dotted line), and H^2_K (dashed line). The exponential growth of $H^2_{\mathcal{N},\mathcal{R},\mathcal{I}}$ effectively fills the Universe with relativistic particles, introducing an instability to the initial de Sitter phase. The right panels illustrate the scale factor $a(t)$ and Hubble parameter $H(t)$ transitioning from a Sitter bounce to a radiation dominated phase. Here the solid lines represent the solutions to the back-reaction problem, while the dashed lines trace the pure de Sitter bounce.

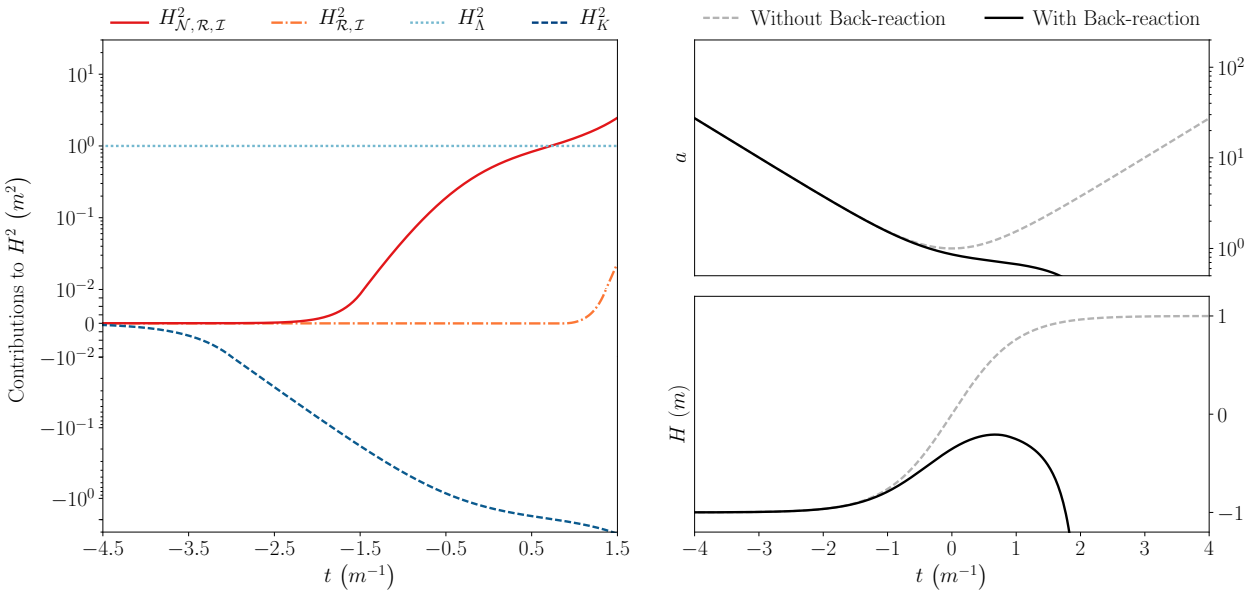

Figure 16: The evolution of every source term featuring on the right-hand side of the semi-classical Friedmann Eq. (3.25a) and the quantities describing the metric evolution in a full back-reacting calculation. The field parameters are set to $m = 0.0145\, m_P$ and $\xi = \frac{1}{6}$, while the cosmological constant and curvature parameter are characterized by $\Lambda = 3\, m^2$ and $K = 1$. The closed de Sitter initial conditions are set at $t_0 = -5\, m^{-1}$, along with an initial particle distribution given by $\mathcal{N}_k(t_0) = 0$. The left panel follows the evolution of $H^2_{\mathcal{N},\mathcal{R},\mathcal{I}}$ (solid line), $H^2_{\mathcal{R},\mathcal{I}}$ (dot-dashed line), H^2_Λ (dotted line), and H^2_K (dashed line). The growth of $H^2_{\mathcal{N},\mathcal{R},\mathcal{I}}$ fills the Universe with just enough relativistic particles to destabilize the initial de Sitter phase. The right panels illustrate the scale factor $a(t)$ and Hubble parameter $H(t)$ transitioning from a de Sitter bounce to a radiation dominated phase. Here the solid lines represent the solutions to the back-reaction problem, while the dashed lines trace the pure de Sitter bounce. Had the field mass been set to a value $m \lesssim 0.0142\, m_P$, a bounce would still take place, albeit at a slightly later time and for a smaller value of the scale factor.

3.7 DISCUSSION

The back-reaction problem addressed in this work imposes several technical hurdles which have resisted a satisfactory solution for decades. These difficulties stem primarily from the necessity to control the divergent nature of the vacuum energy. Adiabatic regularization accomplishes this at the cost of increasing the problem's complexity. As a result, ambiguities arise in the specification of initial conditions and in the value of physical quantities when particle production is rapid, and computationally the problem becomes susceptible to potential numerical instabilities. In this work we have shown that these issues can be circumvented in scenarios dominated by particle production. Our approach relies on a particular choice of adiabatic mode functions which isolate the vacuum contributions into a separate covariantly conserved component of the total stress-energy. In regimes dominated by particle production, this vacuum component is sub-dominant and can be discarded in its entirety. By definition, the remaining covariantly conserved portion of the stress-energy dominates, as it encapsulates the effects of particle production. This component can be expressed in terms of the particle number density as described by Berry's universal form, resolving the ambiguity in physical quantities, and computed from the analytic continuation of each mode's frequency function onto the complex plane (Figures 13 and 14). The resulting stress-energy is a calculable source term for the semi-classical Friedmann equations, and can be used to obtain a numerical solution to the back-reaction problem. We have performed this calculation for an initially closed de Sitter spacetime, demonstrating that the effects of particle production in this scenario can become strong enough to drive the cosmic evolution into a radiation-dominated phase (Figures 15 and 16). Our results illustrate the reliability of our numerical implementation, and open the possibility of the systematic investigation of cosmological scenarios dominated by quantum particle production.

On a technical level, our method relies on some previous knowledge of the Stokes geometry associated with the spacetime evolution. For the case studied in this work, all Stokes lines are sufficiently separated from each other so that Berry's universal form for particle production applies without corrections. In general, however, the spacetime evolution might result in near-lying Stokes lines for which higher-order Stokes corrections are required for an

accurate description of particle production. Although not included in this work, such corrections are well-documented in the literature [109–111] and could in principle be added to our numerical implementation. More fundamentally, our method is based on a well-defined semi-classical notion of particle. Mathematically, this notion is tied to the existence of a phase-integral expansion for the field mode functions. Such a representation can always be constructed as long as $|\varepsilon_{k,0}| \ll 1$. Physically, this requirement typically translates to an approximate bound on the Hubble rate $H \lesssim m$ set by the mass of the field under consideration. Nonetheless, some scenarios exist for which $|\varepsilon_{k,0}| \ll 1$ is satisfied even when $H > m$.

Quantum backreaction is potentially important in models of the very early Universe. Quantum particle production is actually quite familiar in the context of inflation, as it provides the standard mechanism for the generation of perturbations in an inflating spacetime [27, 73–78, 112]. Interestingly, it has been suggested that these same ideas could be applied to the problem of driving inflation itself [113–119]. Indeed, a phase of accelerated expansion can result if particles are produced at a high enough rate. A time derivative of the usual Friedmann Equation $H^2(t) = \frac{1}{3} m_P^{-2} \rho(t)$ shows that an accelerating expansion $\ddot{a} > 0$ occurs when

$$\dot{\rho}(t) > -\frac{2}{\sqrt{3}}\, m_P^{-1} \rho^{3/2}(t)\,. \tag{3.39}$$

Such a scenario has the potential to sidestep some of the conceptual problems of the standard inflationary paradigm. For instance, it has been argued that standard inflation cannot generically start in a patch which is smaller than the cosmological horizon without violating either causality or the weak energy condition [120, 121]. However, if inflation is initially driven by an increasing energy density due to particle production, the weak energy condition *is* effectively violated. Therefore, inflation driven by such a mechanism could generically start in small patches contained within the cosmological horizon without violating causality. Inflation driven by particle production would also clarify the meaning of the inflaton effective potential by making manifest the high mass-scale physics it represents.

The same conditions which lead to quantum particle production can also result in particle annihilation. If sufficiently pronounced, this effect can drive a contracting spacetime toward a bounce phase. Indeed, it follows from the cosmological continuity equation that $\rho(t) + P(t) < 0$ provided the particle annihilation rates are high enough to cause the field

energy density to decrease as the Universe contracts. In other words, the null energy condition is effectively violated, making $\dot{H}(t) > 0$ according to the Friedmann equations [122,123]. Thus, a classical bounce can emerge provided enough energy density is sequestered by quantum particle annihilation during a phase of cosmological contraction. If realized, such a mechanism could provide a natural description for cosmological bounce scenarios which does not require new physics. Also, successful bounces require constraints on high mass-scale quantum fields, so that quantum back-reaction does not push the contracting phase into a radiation crunch, as with the example solved in this paper.

Another possibly interesting effect is the production of a relativistic condensate in the early universe. Under certain circumstances, quantum particle production can lead to large occupation numbers for some scalar field modes, representing condensate formation. This phenomenon could lead to additional interesting phenomenology [124–126].

A number of technical questions remain to be answered. Fermion fields require more complex calculations than scalar fields, and may present some different physics [127, 128]. How to handle interacting fields remains an open question, and multiple fields offer additional possibilities [129–134]. We have a long road to travel before the range of interesting early-Universe dynamical scenarios driven by quantum particle production has been fully explored.

4.0 SUMMARY AND OUTLOOK

In the past decades, cosmological observations have unveiled a spatially flat and statistically isotropic early Universe, filled with primordial perturbations characterized by a nearly scale-invariant power spectrum. In spite of this remarkable progress, the physical mechanism responsible for originating these early conditions remains a subject of ongoing research and debate. In this work, we have employed new computational and mathematical techniques with the goal of further understanding the physics behind the earliest moments of our Universe.

An early inflationary period has been proposed as a possible explanation for the observed large-scale properties of our Universe. It is therefore of interest to place observational constraints on inflationary dynamics in order to better understand its physical origin. Typically, this has been done by forward modeling, i.e., by picking an inflation model and matching its observable consequences to actual measurements. While this approach can rule out many inflation models, it cannot be used to quantify which of the surviving models are more likely. Circumventing this issue requires the solution of the inverse problem, for which the constraints on inflationary history arise directly from measurements. We explored this approach in Chapter 2 by employing quantum mechanical inverse-scattering techniques. The task of inverse-scattering theory is to determine the features of a scattering target from its associated scattering data. In the context of inflation, the inflationary dynamics itself acts as a scattering potential, while the primordial power spectra take on the role of the scattering data. This approach is advantageous in that it is not only independent of any particular model space parameterization, but it also does not require slow-roll conditions to be satisfied. We have demonstrated this inverse procedure for two simulated inflationary histories, assuming perfect knowledge of their corresponding observables. Moving forward,

this calculation can form the basic building block for future model-independent estimation of inflation dynamics from noisy measurements of the primordial scalar and tensor power spectra. The wider the range of scales covered by power spectra measurements, the longer the period of inflationary dynamics that can be recovered. In practice, such measurements might not be accessible at smaller length scales, but having the technology to invert the data in such fashion will allow us to make the most of all future observations constraining primordial perturbations.

In Chapter 3 we have investigated the effects of gravitationally induced quantum particle production on the evolution of cosmological spacetimes. This effect is particularly relevant for models of the very early Universe, when the energy density generated through this process might have come to back-react on the cosmological evolution. Surprisingly, such scenarios remained unexplored for decades due to the several technical hurdles imposed by the back-reaction calculations. In order to tackle this problem, we have employed new mathematical and computational methods to offer a self-consistent formulation and solution to this problem in regimes dominated by particle production. Our approach makes use of a remarkable result from asymptotic theory which allows for an unambiguous notion of particle to be defined on cosmological backgrounds. By numerically tracking the particle number density and cosmological scale factor with a combination of B-spline and finite-difference techniques, we were able to solve for the interplay between particle production and metric evolution. We have demonstrated an application of our algorithm for an initially closed de Sitter spacetime, showing that particle production can drive the cosmic evolution into a radiation dominated phase. Our implementation opens the possibility for the further systematic investigation of cosmological scenarios dominated by quantum particle production. Regimes characterized by high quantum particle production/annihilation rates are of particular interest, as these could lead to an either inflationary or bouncing phase. If realized, such scenarios would provide a specific picture of the physical mechanism underlying the usual effective field approaches used to model the very early Universe. However, a thorough exploration of interesting early-Universe dynamical scenarios driven by quantum particle production will require additional technical challenges to be addressed. These include the proper handling of spinor fields and the formalization of interacting fields on curved spacetimes.

APPENDIX A

THE JOST FUNCTION

The Jost function, $F_\ell(k)$, encapsulates all the information about the scattering problem and therefore plays a central role in the theory of inverse scattering. Its definition is given in terms of two particular sets of solutions for the the radial time-independent Schrödinger equation: the regular solutions, $\varphi_\ell(k,\, r)$; and the Jost solutions, $f_\ell(k,\, r)$. Regular solutions are those satisfying the boundary condition $\lim_{r\to 0}(2\ell+1)!!\, r^{-\ell-1}\varphi_\ell = 1$. The Jost solutions, on the other hand, are those satisfying $\lim_{r\to\infty} e^{-ikr} f_\ell(k,\, r) = 1$. These are used to define the Jost function through the Wronskian

$$F_\ell(k) = (-k)^\ell\, W\Big\{ f_\ell(k,\, r),\, \varphi_\ell(k,\, r) \Big\}\,. \tag{A.1}$$

Taking the limit of this expression for $r \longrightarrow 0$, we obtain [47]

$$F_\ell(k) = \lim_{r\to 0}\left[\frac{e^{-i\pi\ell}\,\Gamma\!\left(\frac{1}{2}\right)}{\Gamma\!\left(\ell+\frac{1}{2}\right)} \left(\frac{kr}{2}\right)^{\ell} f_\ell(k,r) \right]\,. \tag{A.2}$$

In the context of inflationary perturbations, the behavior of the Jost solutions as $\eta \longrightarrow -\infty$ coincides with that of modes set by the Bunch-Davies vacuum. As a consequence, the Jost solutions must behave as $f_\ell(k,\, r) = A_k z$ for $r \longrightarrow 0$. Furthermore, for small r, the effective potential experienced by the scattered particle is mostly due to the centrifugal term $\ell\,(\ell+1)\, r^{-2}$ in the Schrödinger equation (2.2). Therefore, for $r \longrightarrow 0$ the Mukhanov variable must have the form $z = r_0/r^\ell$, where r_0 is a constant. Combining these results with (A.2)

gives the following expression relating the Jost function and A_k:

$$A_k = \frac{\Gamma\left(\ell + \frac{1}{2}\right)}{\pi r_0}\left(\frac{2}{k}\right)^{\ell+\frac{1}{2}} F_\ell(k)\,. \tag{A.3}$$

This expression, along with Eq. (1.44), yields Eq. (2.4) which relates the Jost function to the primordial power spectrum.

APPENDIX B

SOLVING THE GEL'FAND-LEVITAN-MARCHENKO EQUATION

Below we describe the method of separable kernel decomposition for solving the Gel'fand-Levitan-Marchenko equation. We start by assuming that the input kernel, $G(r,\, s)$, can be written as

$$G(r,\, s) = \sum_{i=1}^{m} a_i(r)\, b_i(s)\,, \tag{B.1}$$

where $a_i = j_\ell(rk_i)$ and $b_i = j_\ell(sk_i)\Big[|F_\ell(k_i)|^{-2} - 1\Big]\Delta_i$. Here, Δ_i essentially represents the integration step. For higher numerical resolution $\Delta_i \longrightarrow 0$, and consequently $m \longrightarrow \infty$. Now consider the Gel'fand-Levitan-Marchenko equation:

$$K(r,\, s) + G(r,\, s) + \int_0^r K(r,\, t)\, G(t,\, s)\, \mathrm{d}t = 0\,. \tag{B.2}$$

We can make use of Eq. (B.1) to rewrite it as

$$K(r,\, s) \;=\; -G(r,\, s) - \sum_{i=1}^{m} b_i(s) \int_0^r K(r,\, t)\, a_i(t)\, \mathrm{d}t \tag{B.3}$$

$$K(r,\, s) \;=\; -G(r,\, s) - \sum_{i=1}^{m} b_i(s)\, c_i(r)\,, \tag{B.4}$$

where we have defined

$$c_i(r) \equiv \int_0^r K(r,\, t)\, a_i(t)\, \mathrm{d}t\,. \tag{B.5}$$

Replacing this last expression for $K(r,s)$ in (B.5) we obtain a system of m equations given by

$$c_i(r) = -g_i(r) - \sum_{j=1}^{m} c_j(r)\, h_{ij}(r)\,, \tag{B.6}$$

where we have defined

$$g_i(r) \equiv \int_0^r G(r,\, t)\, a_i(t)\, \mathrm{d}t \tag{B.7}$$

$$h_{ij}(r) \equiv \int_0^r a_i(t)\, b_j(t)\, \mathrm{d}t\,. \tag{B.8}$$

Since $G(r,s)$ is known and both a_i and b_i can be easily computed, the Gel'fand-Levitan-Marchenko equation is reduced to the linear system of equations (B.6). The solutions for $c_i(r)$ can easily be obtained numerically and corresponds to an m-tuple: $(c_1,\, \ldots,\, c_m)$. Substituting this result in Eq. (B.4) gives the desired output kernel $K(r,\, s)$.

APPENDIX C

THE LEVIN METHOD

Here we show the essential results needed for an implementation of the Levin method targeted at computing the oscillatory integral in Eq. (2.6) for the input kernel. For a more detailed explanation of this integration method we refer the reader to the original paper by Levin [54]. Below we follow Levin's notation.

First, we assume that the integral Eq. (2.6) has a solution of the form

$$\int \mathbf{f}(k) \cdot \mathbf{w}(k)\, \mathrm{d}k = \sum_{i}^{m} F_i(k)\, w_i(k), \tag{C.1}$$

where $\mathbf{w}(x)$ is defined to be the vector of length m containing the oscillatory kernel function, and $\mathbf{f}(k)$ is the amplitude function. In our case these are clearly given by

$$\mathbf{w}(k) = \begin{bmatrix} J_\ell(rk)\, J_\ell(sk) \\ J_{\ell-1}(rk)\, J_\ell(sk) \\ J_\ell(rk)\, J_{\ell-1}(sk) \\ J_{\ell-1}(rk)\, J_{\ell-1}(sk) \end{bmatrix} \quad \text{and} \quad \mathbf{f}(k) = \begin{bmatrix} k\Big[|F_\ell(k)|^{-2} - 1\Big] \\ 0 \\ 0 \\ 0 \end{bmatrix}. \tag{C.2}$$

We use a Chebyshev polynomial expansion for the solution function, $F_i(x) = \sum_k^n c_{ik} u_k(x)$. The final step is to compute the $(m \times n)$ c_{ik} coefficients by solving the following ordinary differential equation

$$f_i(x) = F_i'(x) + \sum_{j}^{m} A_{ij}(x)\, F_j(x)\,, \tag{C.3}$$

where the matrix A_{ij} must satisfy the relation $d\mathbf{w}(k)/dk = \mathbf{A}(k)\,\mathbf{w}(k)$. Using the Bessel function recurrence relations, the matrix $\mathbf{A}$ is given by

$$\mathbf{A} = \begin{bmatrix} -\frac{2\ell}{k} & r & s & 0 \\ -r & -\frac{1}{k} & 0 & s \\ -s & 0 & -\frac{1}{k} & r \\ 0 & -s & -r & \frac{2(\ell-1)}{k} \end{bmatrix} . \tag{C.4}$$

Employing these expressions for the Levin's collocation procedure described in [54] allows one to compute the integral in Eq. (2.6). The convergence of this integration method depends roughly on the ratio between the size of the integration range and the n number of collocation points, with better convergence being achieved for smaller values of this ratio.

The accuracy of the inversion procedure is directly affected by step size in the numerical evaluation of the output kernel. More accurate results can be obtained by increasing the numerical resolution in the inversion algorithm, at the cost of increasing the computation time. In our calculations we employ a resolution of 10^4 bins for the smallest logarithmic interval $\left[10^{-6},\, 10^{-5}\right]\,\mathrm{Mpc}^{-1}$ when computing the integral Eq. (2.6) and keep the resolution constant for the rest of the analysis. A more detailed error analysis of the reconstruction will be investigated in a future work.

APPENDIX D

VACUUM REGULARIZATION

In order to avoid the technical difficulties introduced by adiabatic regularization, we employ an alternative scheme which discards the vacuum contributions to the field energy-momentum tensor in their entirety. Albeit cruder, this method yields a good approximation to the field energy density $\rho(t)$ and pressure $P(t)$ in regimes dominated by particle production. Care must be taken, however, to ensure that the resulting expressions for these quantities satisfy the cosmological continuity equation. Below we demonstrate that this can be achieved by selecting an appropriate definition for the adiabatic vacuum.

The residual freedom that exists in the definition of the adiabatic mode functions allows for a slight shift in the balance between particle and vacuum contributions to energy density and pressure expressed in Eqs. (3.27). Although small, this latitude can be exploited to ensure that the vacuum contributions $\rho_{\rm vac}(t)$ and $P_{\rm vac}(t)$ defined by Eqs. (3.29) independently satisfy the cosmological continuity equation.

Underlying this separation between particle and vacuum components are the functions $W_k(t)$ and $V_k(t)$. The first of these is given by the asymptotic series in Eq. (3.2), which is the solution to the differential equation

$$W_k^2(t) = \Omega_k^2(t) + \frac{3}{4}\frac{\dot{W}_k^2(t)}{W_k^2(t)} - \frac{1}{2}\frac{\ddot{W}_k(t)}{W_k(t)}\,, \tag{D.1}$$

obtained from the substitution of Eq. (3.1) into Eq. (1.28). The function $V_k(t)$, on the other hand, encapsulates the remaining freedom in the definition of the adiabatic vacuum, and can

be chosen to have any convenient functional form which satisfies the following constraint:

$$V_k(t) - H(t) < \mathcal{O}(k^{-2}) \quad \text{as} \quad k \longrightarrow \infty \,. \tag{D.2}$$

A natural choice which meets the above requirement is given by

$$V_k(t) = -\frac{\dot{W}_k(t)}{W_k(t)} \,. \tag{D.3}$$

Interestingly, this functional form also guarantees that the vacuum contributions $\rho_{\text{vac}}(t)$ and $P_{\text{vac}}(t)$ satisfy the cosmological continuity equation. It can be verified with the aid of Eqs. (D.1) and (D.3) that

$$\dot{\rho}_{\text{vac}}(t) = -3H(t)\Big[\rho_{\text{vac}}(t) + P_{\text{vac}}(t)\Big] \,, \tag{D.4}$$

where the right-hand side follows from the left-hand side by explicit calculation. It is worth noting that this result is valid for all truncation orders of $W_k(t)$ as given by Eq. (3.2).

Hence, provided the function $V_k(t)$ has the form established in Eq. (D.3), it follows directly from Eqs. (3.26) and (D.4) that the vacuum and particle contributions to the field energy density and pressure independently satisfy the cosmological continuity equation.

BIBLIOGRAPHY

[1] C. W. Misner, K. S. Thorne, J. A. Wheeler, and D. I. Kaiser. *Gravitation*. Princeton University Press, 2017.

[2] R. M. Wald. *General Relativity*. University of Chicago Press, 1984.

[3] S. M. Carroll. *Spacetime and Geometry. An introduction to General Relativity*. Pearson, 2004.

[4] E. W. Kolb and M. S. Turner. *The Early Universe*. Addison-Wesley, 1990.

[5] S. Dodelson. *Modern cosmology*. Elsevier, 2003.

[6] S. Weinberg. *Cosmology*. Oxford University Press, 2008.

[7] N. D. Birrell and P. C. W. Davies. *Quantum fields in curved space*. Cambridge University Press, 1984.

[8] L. Parker and D. Toms. *Quantum field theory in curved spacetime: quantized fields and gravity*. Cambridge University Press, 2009.

[9] P. A. R. Ade et al. Planck 2015 results XIII: Cosmological parameters. *Astron. Astrophys.*, 594:A13, 2016.

[10] C. L. Bennett et al. Nine-year Wilkinson microwave anisotropy probe (WMAP) observations: final maps and results. *Astrophys. J.*, 208:20, 2013.

[11] P. Sarkar, J. Yadav, B. Pandey, and S. Bharadwaj. The scale of homogeneity of the galaxy distribution in SDSS DR6. *Mon. Notices Royal Astron. Soc. Lett.*, 399:L128–L131, 2009.

[12] G. E. Addison, G. Hinshaw, and M. Halpern. Cosmological constraints from baryon

acoustic oscillations and clustering of large-scale structure. *Mon. Notices Royal Astron. Soc.*, 436:1674–1683, 2013.

[13] D. Clowe, A. Gonzalez, and M. Markevitch. Weak-lensing mass reconstruction of the interacting cluster 1e 0657–558: Direct evidence for the existence of dark matter. *Astrophys. J.*, 604:596, 2004.

[14] D. Coe, N. Benítez, T. Broadhurst, and L. A. Moustakas. A high-resolution mass map of galaxy cluster substructure: LensPerfect analysis of A1689. *Astrophys. J.*, 723:1678, 2010.

[15] R. Adam et al. Planck 2015 results I: Overview of products and scientific results. *Astron. Astrophys.*, 594:A1, 2016.

[16] A. M. Boesgaard and G. Steigman. Big Bang nucleosynthesis: theories and observations. *Ann. Rev. Astron. Astrophys.*, 23:319–378, 1985.

[17] R. Durrer. *The Cosmic Microwave Background*. Cambridge University Press, 2008.

[18] A. Loeb and R. Barkana. The reionization of the universe by the first stars and quasars. *Ann. Rev. Astron. Astrophys.*, 39:19–66, 2001.

[19] F. Combes, P. Boissé, A. Mazure, and A. Blanchard. *Galaxies and Cosmology*. Springer Science & Business Media, 2004.

[20] A. Riess, A. V. Filippenko, P. Challis, A. Clocchiatti, A. Diercks, P. M. Garnavich, R. L. Gilliland, C. J. Hogan, S. Jha, R. P. Kirshner, et al. Observational evidence from supernovae for an accelerating universe and a cosmological constant. *Astron. J.*, 116:1009, 1998.

[21] J. Magueijo and K. Baskerville. Big Bang riddles and their revelations. *Philos. Trans. Royal Soc.*, 357:3221–3236, 1999.

[22] A. H. Guth. The inflationary universe: A possible solution to the horizon and flatness problems. *Phys. Rev. D*, 23:347–356, 1981.

[23] K. Sato. First order phase transition of a vacuum and expansion of the universe. *Mon. Notices Royal Astron. Soc.*, 195:467–479, 1981.

[24] W. H. Kinney. TASI lectures on inflation. *arXiv:0902.1529*, 2009.

[25] A. R. Liddle and S. M. Leach. How long before the end of inflation were observable perturbations produced? *Phys. Rev. D*, 68:103503, 2003.

[26] J. M. Bardeen. Gauge-invariant cosmological perturbations. *Phys. Rev. D*, 22:1882, 1980.

[27] V. F. Mukhanov, H. A. Feldman, and R. H. Brandenberger. Theory of cosmological perturbations. *Phys. Rep.*, 215:203–333, 1992.

[28] V. F. Mukhanov. Quantum theory of gauge-invariant cosmological perturbations. *Zh. Eksp. Teor. Fiz*, 94, 1988.

[29] M. Sasaki. Large scale quantum fluctuations in the inflationary universe. *Prog. Theor. Phys.*, 76:1036–1046, 1986.

[30] D. Baumann. TASI lectures on inflation. *arXiv:0907.5424*, 2009.

[31] Keck Array and BICEP2 Collaborations, P. A. R. Ade, et al. Improved constraints on cosmology and foregrounds from BICEP2 and Keck Array cosmic microwave background data with inclusion of 95 GHz band. *Phys. Rev. Lett.*, 116:031302, 2016.

[32] Y. Akrami et al. Planck 2018 results X: Constraints on inflation. *arXiv:1807.06211*, 2018.

[33] A. D. Linde. Inflationary cosmology. *Lect. Notes Phys.*, 738:1–54, 2008.

[34] P. A. R. Ade et al. Planck 2015 results XX: Constraints on inflation. 2015.

[35] J. Caligiuri, A. Kosowsky, W. H. Kinney, and N. Seto. Constraining the history of inflation from microwave background polarimetry and laser interferometry. *Phys. Rev. D*, 91:103529, 2015.

[36] R. Hlozek, J. Dunkley, , G. Addison, J. W. Appel, J. R. Bond, et al. The Atacama Cosmology Telescope: a measurement of the primordial power spectrum. *Astrophys. J.*, 749:90, 2012.

[37] J. Caligiuri and A. Kosowsky. Inflationary tensor perturbations after BICEP2. *Phys. Rev. Lett.*, 112:191302, 2014.

[38] E. J. Copeland, I. J. Grivell, E. W. Kolb, and A. R. Liddle. On the reliability of inflaton potential reconstruction. *Phys. Rev. D*, 58:043002, 1998.

[39] P. J. Steinhardt and M. S. Turner. A prescription for successful new inflation. *Phys. Rev. D*, 29:2162–2171, 1984.

[40] H. P. de Oliveira and C. A. Terrero-Escalante. Troubles for observing the inflaton potential. *JCAP*, 0601:024, 2006.

[41] W. H. Kinney. Inflation: Flow, fixed points and observables to arbitrary order in slow roll. *Phys. Rev. D*, 66:083508, 2002.

[42] S. Habib, K. Heitmann, and G. Jungman. Inverse-scattering theory and the density perturbations from inflation. *Phys. Rev. Lett.*, 94:061303, 2005.

[43] I. M. Gel'fand and B. M. Levitan. On the determination of a differential equation from its spectral function. *Izv. Akad. Nauk SSSR Ser. Mat.*, 15:309–360, 1951.

[44] V. A. Marchenko. On reconstruction of the potential energy from phases of the scattered waves. *Dokl. Akad. Nauk SSSR*, 104:695–698, 1955.

[45] V. A. Marchenko. *Sturm-Liouville Operators and Applications*. American Mathematical Society, 2011.

[46] R. G. Newton. *Scattering Theory of Waves and Particles*. Dover Publications, 1982.

[47] R. G. Newton, K. Chadan, and P. C. Sabatier. *Inverse Problems in Quantum Scattering Theory*. Springer Berlin Heidelberg, 2011.

[48] J. F. Moser and H. P. Baltes. *Inverse Source Problems in Optics*. Springer Berlin Heidelberg, 2011.

[49] M. J. Ablowitz and H. Segur. *Solitons and the Inverse Scattering Transform*. SIAM Philadelphia, 1981.

[50] J. Adams, B. Cresswell, and R. Easther. Inflationary perturbations from a potential with a step. *Phys. Rev. D*, 64:123514, 2001.

[51] C. R. Keeton and L. A. Moustakas. A new channel for detecting dark matter substructure in galaxies: Gravitational lens time delays. *Astrophys. J.*, 699:1720, 2009.

[52] W. H. W. Ngan and R. G. Carlberg. Using gaps in N-body tidal streams to probe missing satellites. *Astrophys. J.*, 788:181, 2014.

[53] J. Chluba, A. L. Erickcek, and I. Ben-Dayan. Probing the inflaton: Small-scale power spectrum constraints from measurements of the CMB energy spectrum. *Astrophys. J.*, 758:76, 2012.

[54] D. Levin. Fast integration of rapidly oscillatory functions. *J. Comp. Appl. Math.*, 67:95–101, 1996.

[55] C. Sealfon, L. Verde, and R. Jimenez. Smoothing spline primordial power spectrum reconstruction. *Phys. Rev. D*, 72:103520, 2005.

[56] L. Verde and H. V. Peiris. On minimally-parametric primordial power spectrum reconstruction and the evidence for a red tilt. *JCAP*, 0807:009, 2008.

[57] Zong-Kuan Guo, D. J. Schwarz, and Yuan-Zhong Zhang. Reconstruction of the primordial power spectrum from CMB data. *JCAP*, 1108:031, 2011.

[58] B. Hu, Jian-Wei Hu, Zong-Kuan Guo, and Rong-Gen Cai. Reconstruction of the primordial power spectra with Planck and BICEP2 data. *Phys. Rev. D*, 90:023544, 2014.

[59] J. A. Vazquez, M. Bridges, M. P. Hobson, and A. N. Lasenby. Model selection applied to reconstruction of the primordial power spectrum. *JCAP*, 1206:006, 2012.

[60] M. S. Turner. Detectability of inflation produced gravitational waves. *Phys. Rev. D*, D55:435–439, 1997.

[61] L. Parker. Quantized fields and particle creation in expanding universes I. *Phys. Rev.*, 183:1057, 1969.

[62] L. Parker. Quantized fields and particle creation in expanding universes II. *Phys. Rev. D*, 3:346, 1971.

[63] Y. B. Zeldovich and A. A. Starobinsky. Rate of particle production in gravitational fields. *JETP Lett.*, 26, 1977.

[64] S. W. Hawking. Particle creation by black holes. *Comm. Math. Phys.*, 43:199–220,

1975.

[65] W. G. Unruh. Notes on black-hole evaporation. *Phys. Rev. D*, 14:870, 1976.

[66] P. C. W. Davies, S. A. Fulling, and W. G. Unruh. Energy-momentum tensor near an evaporating black hole. *Phys. Rev. D*, 13:2720, 1976.

[67] D. N. Page. Thermal stress tensors in static Einstein spaces. *Phys. Rev. D*, 25:1499, 1982.

[68] M . R. Brown, A. C. Ottewill, and D. N. Page. Conformally invariant quantum field theory in static Einstein space-times. *Physical Review D*, 33:2840, 1986.

[69] V. P. Frolov and A. I. Zel'nikov. Killing approximation for vacuum and thermal stress-energy tensor in static space-times. *Phys. Rev. D*, 35:3031, 1987.

[70] P. R. Anderson, W. A. Hiscock, and D. A. Samuel. Stress-energy tensor of quantized scalar fields in static black hole spacetimes. *Phys. Rev. Lett.*, 70:1739, 1993.

[71] P. R. Anderson, W. A. Hiscock, J. Whitesell, and J. W. York Jr. Semiclassical black hole in thermal equilibrium with a nonconformal scalar field. *Phys. Rev. D*, 50:6427, 1994.

[72] P. R. Anderson, W. A. Hiscock, and D. J. Loranz. Semiclassical stability of the extreme Reissner-Nordström black hole. *Phys. Rev. Lett.*, 74:4365, 1995.

[73] A. A. Starobinsky. Relic gravitation radiation spectrum and initial state of the universe. *JETP Lett.*, 30:131–132, 1979.

[74] B. Allen. Stochastic gravity-wave background in inflationary-universe models. *Phys. Rev. D*, 37:2078, 1988.

[75] V. Sahni. Energy density of relic gravity waves from inflation. *Phys. Rev. D*, 42:453, 1990.

[76] T. Souradeep and V. Sahni. Density perturbations, gravity waves and the cosmic microwave background. *Mod. Phys. Lett. A*, 7:3541–3551, 1992.

[77] M. M. Glenz and L. Parker. Study of the spectrum of inflaton perturbations. *Phys. Rev. D*, 80:063534, 2009.

[78] I. Agullo and L. Parker. Non-gaussianities and the stimulated creation of quanta in the inflationary universe. *Phys. Rev. D*, 83:063526, 2011.

[79] L. Parker and S. A. Fulling. Adiabatic regularization of the energy-momentum tensor of a quantized field in homogeneous spaces. *Phys. Rev. D*, 9:341, 1974.

[80] S. A. Fulling and L. Parker. Renormalization in the theory of a quantized scalar field interacting with a Robertson-Walker spacetime. *Ann. Phys.*, 87:176–204, 1974.

[81] T. S. Bunch. Adiabatic regularization for scalar fields with arbitrary coupling to the scalar curvature. *J. Phys. A*, 13:1297, 1980.

[82] S. A. Fulling, L. Parker, and B. L. Hu. Conformal energy-momentum tensor in curved spacetime: Adiabatic regularization and renormalization. *Phys. Rev. D*, 10:3905, 1974.

[83] S. M. Christensen. Regularization, renormalization, and covariant geodesic point separation. *Phys. Rev. D*, 17:946, 1978.

[84] P. R. Anderson and L. Parker. Adiabatic regularization in closed Robertson-Walker universes. *Phys. Rev. D*, 36:2963, 1987.

[85] P. R. Anderson. Effects of quantum fields on singularities and particle horizons in the early universe. *Phys. Rev. D*, 28:271, 1983.

[86] P. R. Anderson. Effects of quantum fields on singularities and particle horizons in the early universe II. *Phys. Rev. D*, 29:615, 1984.

[87] P. R. Anderson. Effects of quantum fields on singularities and particle horizons in the early universe III: The conformally coupled massive scalar field. *Phys. Rev. D*, 32:1302, 1985.

[88] P. R. Anderson. Effects of quantum fields on singularities and particle horizons in the early universe IV: Initially empty universes. *Phys. Rev. D*, 33:1567, 1986.

[89] Wai-Mo Suen and P. R. Anderson. Reheating in the higher-derivative inflationary models. *Phys. Rev. D*, 35:2940, 1987.

[90] N. D. Birrell. The application of adiabatic regularization to calculations of cosmological interest. *Proc. R. Soc. Lond. A*, 361:513–526, 1978.

[91] P. R. Anderson, W. Eaker, S. Habib, C. Molina-Paris, and E. Mottola. Attractor states and infrared scaling in de Sitter space. *Phys. Rev. D*, 62:124019, 2000.

[92] P. R. Anderson, C. Molina-Paris, and E. Mottola. Short distance and initial state effects in inflation: Stress tensor and decoherence. *Phys. Rev. D*, 72:043515, 2005.

[93] J. D. Bates and P. R. Anderson. Effects of quantized scalar fields in cosmological spacetimes with Big Rip singularities. *Phys. Rev. D*, 82:024018, 2010.

[94] S. Habib, C. Molina-Paris, and E. Mottola. Energy-momentum tensor of particles created in an expanding universe. *Phys. Rev. D*, 61:024010, 1999.

[95] P. R. Anderson and E. Mottola. Instability of global de Sitter space to particle creation. *Phys. Rev. D*, 89:104038, 2014.

[96] P. R. Anderson and E. Mottola. Quantum vacuum instability of "eternal" de Sitter space. *Phys. Rev. D*, 89:104039.

[97] P. R. Anderson, E. Mottola, and D. H. Sanders. Decay of the de Sitter vacuum. *Phys. Rev. D*, 97:065016, 2018.

[98] R. Dabrowski and G. V. Dunne. Superadiabatic particle number in Schwinger and de Sitter particle production. *Phys. Rev. D*, 90:025021, 2014.

[99] R. Dabrowski and G. V. Dunne. Time dependence of adiabatic particle number. *Phys. Rev. D*, 94:065005, 2016.

[100] R. B. Dingle. *Asymptotic expansions: their derivation and interpretation.* Academic Press London, 1973.

[101] M. V. Berry. Waves near Stokes lines. *Proc. R. Soc. Lond. A*, 427:265–280, 1990.

[102] M. V. Berry. Semiclassically weak reflections above analytic and non-analytic potential barriers. *J. Phys. A*, 15:3693, 1982.

[103] M. V. Berry. Uniform asymptotic smoothing of Stokes's discontinuities. *Proc. R. Soc. Lond. A*, 422:7–21, 1989.

[104] M. V. Berry. Stokes' phenomenon: smoothing a Victorian discontinuity. *Pub. Math. de l'IHÉS*, 68:211–221, 1988.

[105] N. Fröman and P. O. Fröman. *Phase-integral method: allowing nearlying transition points*. Springer Science & Business Media, 2013.

[106] N. Fröman and P. O. Fröman. *Physical problems solved by the phase-integral method*. Cambridge University Press, 2002.

[107] C. M. Bender and S. A. Orszag. *Advanced mathematical methods for scientists and engineers I: Asymptotic methods and perturbation theory*. Springer Science & Business Media, 2013.

[108] E. Mottola. Particle creation in de Sitter space. *Phys. Rev. D*, 31:754, 1985.

[109] M. V. Berry and C. J. Howls. Overlapping Stokes smoothings: survival of the error function and canonical catastrophe integrals. *Proc. R. Soc. Lond. A*, 444:201–216, 1994.

[110] C. J. Howls, P. J. Langman, and A. B. Olde Daalhuis. On the higher-order Stokes phenomenon. *Proc. R. Soc. Lond. A*, 460:2285–2303, 2004.

[111] C. J. Howls and A. B. Olde Daalhuis. Exponentially accurate solution tracking for nonlinear ODEs, the higher order Stokes phenomenon and double transseries resummation. *Nonlinearity*, 25:1559, 2012.

[112] V. Sahni and S. Habib. Does inflationary particle production suggest $\Omega_m < 1$? *Phys. Rev. Lett.*, 81:1766, 1998.

[113] I. Prigogine. Thermodynamics and cosmology. *Int. J. of Theor. Phys.*, 28:927–933, 1989.

[114] M. O. Calvao, J. A. S. Lima, and I. Waga. On the thermodynamics of matter creation in cosmology. *Phys. Lett. A*, 162:223–226, 1992.

[115] J. A. S. Lima, A. S. M. Germano, and L. R. W. Abramo. FRW-type cosmologies with adiabatic matter creation. *Phys. Rev. D*, 53:4287, 1996.

[116] L. R. W. Abramo and J. A. S. Lima. Inflationary models driven by adiabatic matter creation. *Class. Quant. Grav.*, 13:2953, 1996.

[117] E. Gunzig, R. Maartens, and A. V. Nesteruk. Inflationary cosmology and thermody-

namics. *Class. Quant. Grav.*, 15:923, 1998.

[118] J. A. S. Lima and I. Baranov. Gravitationally induced particle production: Thermodynamics and kinetic theory. *Phys. Rev. D*, 90:043515, 2014.

[119] J. de Haro and S. Pan. Gravitationally induced adiabatic particle production: from Big Bang to de Sitter. *Class. Quant. Grav.*, 33:165007, 2016.

[120] T. Vachaspati and M. Trodden. Causality and cosmic inflation. *Phys. Rev. D*, 61:023502, 1999.

[121] A. Berera and C. Gordon. Inflationary initial conditions consistent with causality. *Phys. Rev. D*, 63:063505, 2001.

[122] A. Ijjas and P. J. Steinhardt. Bouncing cosmology made simple. *Class. Quant. Grav.*, 35:135004, 2018.

[123] A. Ijjas, J. Ripley, and P. J. Steinhardt. NEC violation in mimetic cosmology revisited. *Phys. Lett. B*, 760:132–138, 2016.

[124] C. A. de Carvalho and S. G. Rosa Jr. The relativistic bose gas. *J. Phys. A*, 13:3233, 1980.

[125] L. Parker and Y. Zhang. Ultrarelativistic Bose-Einstein condensation in the Einstein universe and energy conditions. *Phys. Rev. D*, 44:2421, 1991.

[126] L. Parker and Y. Zhang. Relativistic condensate as a source for inflation. *Phys. Rev. D*, 47:416, 1993.

[127] A. Landete, J. Navarro-Salas, and F. Torrenti. Adiabatic regularization for spin-1/2 fields. *Phys. Rev. D*, 88:061501, 2013.

[128] A. Landete, J. Navarro-Salas, and F. Torrenti. Adiabatic regularization and particle creation for spin one-half fields. *Phys. Rev. D*, 89:044030, 2014.

[129] A. Ringwald. Evolution equation for the expectation value of a scalar field in spatially flat RW universes. *Ann. of Phys.*, 177:129–166, 1987.

[130] F. Cooper and E. Mottola. Initial-value problems in quantum field theory in the large-N approximation. *Phys. Rev. D*, 36:3114, 1987.

[131] J. P. Paz and F. D. Mazzitelli. Renormalized evolution equations for the back-reaction problem with a self-interacting scalar field. *Phys. Rev. D*, 37:2170, 1988.

[132] S. Habib, Y. Kluger, E. Mottola, and J. P. Paz. Dissipation and decoherence in mean field theory. *Phys. Rev. Lett.*, 76:4660, 1996.

[133] F. Cooper, S. Habib, Y. Kluger, and E. Mottola. Nonequilibrium dynamics of symmetry breaking in $\lambda\varphi^4$ theory. *Phys. Rev. D*, 55:6471, 1997.

[134] C. Molina-Paris, P. R. Anderson, and S. A. Ramsey. One-loop $\lambda\varphi^4$ field theory in Robertson-Walker spacetimes: Adiabatic regularization and analytic approximations. *Phys. Rev. D*, 61:127501, 2000.